algorithms

MDPI

Article

Optimized Analytical–Numerical Procedure for Ultrasonic Sludge Treatment for Agricultural Use

Filippo Laganà [1], Salvatore A. Pullano [1], Giovanni Angiulli [2] and Mario Versaci [3,*]

[1] Department of Health Science, Magna Græcia University, I-88100 Catanzaro, Italy; filippo.lagana@unicz.it (F.L.); pullano@unicz.it (S.A.P.)
[2] Department of Information Engineering, Infrastructures and Sustainable Energy, Mediterranea University, via Zehender, I-89122 Reggio Calabria, Italy; giovanni.angiulli@unirc.it
[3] Department of Civil, Energetic, Environmental and Material Engineering, Mediterranea University, via Zehender, I-89122 Reggio Calabria, Italy
* Correspondence: mario.versaci@unirc.it

Abstract: This paper presents an integrated approach based on physical–mathematical models and numerical simulations to optimize sludge treatment using ultrasound. The main objective is to improve the efficiency of the purification system by reducing the weight and moisture of the purification sludge, therefore ensuring regulatory compliance and environmental sustainability. A coupled temperature–humidity model, formulated by partial differential equations, describes materials' thermal and water evolution during treatment. The numerical resolution, implemented by the finite element method (FEM), allows the simulation of the system behavior and the optimization of the operating parameters. Experimental results confirm that ultrasonic treatment reduces the moisture content of sludge by up to 20% and improves its stability, making it suitable for agricultural applications or further treatment. Functional controls of sonication and the reduction of water content in the sludge correlate with the obtained results. Ultrasound treatment has been shown to decrease the specific weight of the sludge sample both in pretreatment and treatment, therefore improving stabilization. In various experimental conditions, the weight of the sludge is reduced by a maximum of about 50%. Processed sludge transforms waste into a resource for the agricultural sector. Treatment processes have been optimized with low-energy operating principles. Additionally, besides utilizing energy-harvesting technology, plant operating processes have been optimized, accounting for approximately 55% of the consumption due to the aeration of active sludge. In addition, an extended analysis of ultrasonic wave propagation is proposed.

Keywords: sludge treatment for agricultural uses; ultrasound; coupled temperature–humidity–pressure analytical model; FEM analysis

Academic Editors: Dunhui Xiao and Shuai Li

Received: 28 November 2024
Revised: 18 December 2024
Accepted: 19 December 2024
Published: 21 December 2024

Citation: Laganà, F.; Pullano, S.A.; Angiulli, G.; Versaci, M. Optimized Analytical–Numerical Procedure for Ultrasonic Sludge Treatment for Agricultural Use. *Algorithms* **2024**, *17*, 592. https://doi.org/10.3390/a17120592

1. Introduction

The adoption of circular business practices is revolutionizing production and consumption patterns, including integrating water services to promote a sustainable and innovative approach. In the waste management and water treatment system, sewage sludge derived from municipal waste requires resources, high costs, and specific procedures for its treatment, being a complex by-product to dispose or manage [1]. However, when reused circularly to extract materials useful to the community, such sludge can be transformed from a liability into a resource. Being composed of carbon (25–35%), nitrogen (4–5%), phosphorus (2–3%), and oxygen (20–25%), along with traces of other useful constituents, reference [2] dry sludge from wastewater treatment has considerable potential for

use in agriculture [3–7]. In addition, digestate (the organic residue produced by anaerobic digestion) can be used to improve soil properties and is an excellent source of organic fertilizer, contributing to the nutritional needs of crops while also contributing to the long-term sustainable growth of agriculture [8–11]. Due to the presence of contaminants, such as heavy metals, drugs, microplastics, or flame retardants, the potential use of sludge in agriculture applications is often limited [12,13]. Thus, there is a growing interest in improving contaminant extraction to address resource recovery and pollution prevention in sewage sludge management [12,13]. Untreated sludge has a complex structure and high moisture content, with particles retaining water. Reducing the water content results in a smaller sludge volume for transport and disposal; accordingly, drying becomes a critical step in sludge treatment, lowering its transport and disposal costs. Conditioning facilitates water removal, making dehydration and drying faster and less expensive. Without proper conditioning, these processes would require more resources, making them less sustainable and effective. Recent studies have explored different methods of sludge conditioning using various techniques to improve the effectiveness of treatment [14,15]. A relatively simple technique that can be integrated with other treatment systems, now well established in the literature, is based on physical conditioning that applies mechanical forces to sludge to change its structure and facilitate dewatering and removal of contaminants [16]. While this technique reduces the viscosity of the material and improves drying, it requires large amounts of energy and expensive specialized equipment. However, physical conditioning can be ineffective for some types of sludge, especially in the presence of fine particles or chemical contaminants that require more specific treatments [17,18]. Then, we are helped it their removal by sonication using high-frequency compression and rarefaction sound waves, which create bubbles in the liquid that, when they collapse, cause intense forces that disintegrate the sludge particles and facilitate the release of intracellular and extracellular materials [19]. This technique improves dewatering efficiency by increasing sludge biodegradability, resulting in rapid completion of anaerobic digestion [20,21]. In addition, sonication is particularly effective in reducing viscosity and making the sludge more straightforward to process in subsequent stages. However, the high-energy requirements and the need for sophisticated instrumentation and calibration make this method not always advantageous. In addition, the effectiveness of sonication can be limited by specific characteristics of the sludge, such as the presence of substances resistant to cavitation (the collapse of tiny bubbles that transmit significant mechanical forces to the solid material in suspension), making it less effective in some contexts [22,23]. In addition to the above procedure, a less costly method, the hydrodynamic cavitation, can be used for the same purposes. This method takes advantage of the formation and subsequent collapse of microbubbles of steam in a fluid, creating intense forces that break up the particles in the sludge. Specifically, when liquid passes through a constriction or valve at high velocity, it makes a low-pressure zone that induces bubble formation. The collapse of the bubbles releases enough energy to break down cellular structures and facilitate the solubilization of organic materials. While this technique reduces particle size with low energy consumption and less expensive equipment, it is poorly applicable to high-density slurries and is subject to wear of parts exposed to cavitation [24,25]. Also, intensive heat treatment, which produces sludge dewatering by destroying pathogens, is possible; however, the high energy consumption and possible loss of essential elements limit its use [26,27]. Another technique well established in the literature for dewatering and breaking down sludge structures is microwaves, which provide selective, rapid, and uniform heating while reducing treatment time but require expensive equipment without preventing or limiting the formation of unpleasant odors or toxic compounds [28,29]. As far as contaminant removal is concerned, the application of a suitable electric current to the (very dense and highly conductive) sludge, which, by

weakening the binding forces between the particles, helps to separate the solid particles from the aqueous phase, thus reducing the use of any chemical agents [30,31]. Suppose the objective is the degradation of organic matter in low-density sludge. In that case, we are helped by photoanalytical treatment, in which the sludge is exposed to a suitable source of light (constant and prolonged), aided using specific catalysts (usually titanium dioxide) capable of reducing harmful organic compounds and pathogens. However, the continuous exposure to light and the use of expensive catalysts limit its applicability [32,33]. In order to degradate the organic matter in low-density sludge, the photoanalytical treatment can be used. In this case, the sludge is exposed to a suitable source of light (constant and prolonged), aided using specific catalysts (usually titanium dioxide) capable of reducing harmful organic compounds and pathogens [32,33]. Widespread is the mixing of sludge with flocculants/coagulants, which aggregate the particles to form heavy agglomerates that precipitate to the bottom of the tank and rapidly promote dewatering. However, such chemicals are often expensive and produce residues that require further treatment [33–35]. Studies have investigated the combined use of US and ozone to improve sludge conditioning and increase dewatering. Ozone, which is a powerful oxidant, facilitates the rupture of cell membranes and the solubilization of organic matter, therefore enhancing the effect of ultrasound. This combination reduces the sludge's viscosity and its filtration resistance [36]. Other studies have focused on the use of cationic polymers that, when combined with sonication, reduce the concentration of heavy metals and limit the time for sludge conditioning by making them stable during dewatering [15]. Again, the combination of thermo-alkaline conditioning with sonication assists in the degradation of complex organic compounds (due to high temperatures and high pH), facilitating the dewatering of the sludge. The use of ultrasound promotes further solubilization of the compounds and reduces the viscosity of the sludge [37,38]. There is no lack of significant studies on the combined use of microwaves (as a heat source), which can increase the permeability of cell membranes, with ultrasound, which, by causing cavitation, destroys cellular structures and significantly biodegrades sludge [39]. Recently, the combination of ultrasonic techniques with electrocoagulation has been successfully used to remove heavy metals from sludge. Electrical charges destabilize suspended particles, while sonication breaks down cellular structures, facilitating sedimentation of the sludge [40]. These studies strongly suggest that a major line of research must be based on using sonication in combination with chemical or physical treatments to improve sludge quality and manageability significantly. Indeed, combined sonication methods show superior results compared to single treatments, positively impacting process efficiency. Research in this field constantly evolves, with the intent to develop increasingly efficient, sustainable, and environmentally friendly conditioning techniques.

This work introduces an innovative approach that combines sonication with thermal treatment, proposing an advanced physical–mathematical model that couples the thermal and ultrasonic aspects. Such a model allows the reconstruction of detailed maps of temperature, humidity, and pressure on the walls of the treatment tank, providing an accurate and predictive view of system behavior throughout the sludge processing. Integrating this information enables optimized and scientifically based treatment management, reducing operating time and costs. The design of the apparatus was preceded by a detailed numerical simulation using the finite element method (FEM), which allowed the functional characteristics of the tank to be developed and verified virtually, ensuring efficient management of thermal and water variables [41]. The entire apparatus was built and tested only after this software validation, demonstrating complete adherence to regulatory standards for sludge use in agriculture. The proposed system, through integrated sensor monitoring and optimization of operating parameters, has shown the ability to reduce heavy metal content and improve the organic composition of sludge, making it fully compatible with

current environmental requirements. The combined drying and sonication technique also enables particle size reduction of up to 50%, contributing to the sustainability and reuse of materials within a circular economy model [42]. This approach emerges as a practical and innovative model of sustainable sewage sludge management, with results that improve environmental and energy efficiency and demonstrate the possibility of valorizing sludge as a safe and certified agricultural resource.

For completeness, with the aim to provide the reader with a comprehensive overview of related work to the present research, we refer to some scientific studies on innovative sludge treatment and valorization techniques, focusing on sustainable methods, advanced technologies, and energy and nutrient recovery processes. Prominent among them are: (a) work on C recovery for bioenergy and N and P recovery for nutrients [43]; (b) on resource recovery for biogas production and P extraction for agricultural reuse [44]; (c) Anaerobic digestion combined with phosphorus recovery from sludge [45]; (d) Chemical/electrochemical methods for removal of heavy metals [46]; (e) Use of thermolysis and sonication for biogas production [47]; (f) on biochar production and C sequestration [48]; (g) on the use of electrodehydration to improve water removal [49]; (h) on the use of phytoremediation to remove heavy metals [50]; (i) the joint use of microwaves and chemical treatments to reduce pathogens in sludge and recover P and N [51]; (l) waste-to-energy for energy resources [52]; (m) hydrothermal carbonization for biofuel production, nutrient recovery, and energy enhancement [53].

The various sludge treatment techniques discussed above, including physical, thermal, chemical, and combined approaches, each present specific advantages and limitations depending on the context of the application. For clarity and to provide a comprehensive overview, the key characteristics, benefits, and limitations of these techniques are summarized in Table 1.

Table 1. Summary of the main sludge treatment techniques, highlighting their key characteristics, advantages, and limitations to provide a comprehensive overview of their applicability and effectiveness in sludge management.

Technique	Main Characteristics	Advantages	Limitations
Physical conditioning	Application of mechanical forces to alter sludge structure and facilitate dewatering.	Reduces sludge viscosity; improves drying.	High energy consumption; ineffective for fine particles.
Sonication	Use of ultrasonic waves to generate cavitation, breaking down particles and structures.	Increases organic material availability; facilitates dewatering.	High energy requirements; less effective for cavitation-resistant sludge.
Hydrodynamic cavitation	Creation and collapse of microbubbles through high-speed fluid flow in low-pressure zones.	Low energy consumption; inexpensive equipment.	Limited applicability to high-density sludge; mechanical wear.
Thermal treatment	Heat application to destroy pathogens and promote sludge dewatering.	Effective pathogen removal; facilitates dewatering.	High energy consumption; potential loss of essential elements.

Table 1. *Cont.*

Technique	Main Characteristics	Advantages	Limitations
Microwave treatment	Selective, rapid, and uniform heating via electromagnetic waves.	Uniform heating; reduces treatment time.	High equipment cost; potential odor/toxic compound formation.
Electrocoagulation	Use of electric current to destabilize particles, separating solids from the aqueous phase.	Reduces chemical agents use; effective for conductive sludge.	Limited to conductive sludge; moderate energy costs.
Photoanalytical treatment	Light exposure with catalysts (e.g., TiO_2) to degrade harmful organic compounds.	Removes pathogens and harmful compounds; reduces organic matter.	High catalyst cost; prolonged treatment time required.
Flocculation Coagulation	Addition of chemical agents to aggregate particles, promoting rapid sedimentation.	Facilitates quick dewatering; simple implementation.	High reagent costs; generates secondary residues.
Ozone treatment	Use of ozone to oxidize cell membranes and solubilize organic matter.	Reduces viscosity; enhances sonication efficiency.	High operational costs; complex maintenance.
Thermo-alkaline conditioning	Combination of heat and alkaline treatment to degrade complex organic compounds.	Facilitates solubilization and viscosity reduction.	Requires high temperatures and pH; high energy consumption.
Combined techniques	Integration of sonication with other treatments (e.g., microwaves, ozone, thermo-alkaline).	Enhances overall treatment efficiency.	Increased operational costs and complexity compared to single methods.

The remainder of the paper is organized as follows: the description of the sample-based sonication technique is given in Section 2. The proposed procedure to enable the production of sludge for agricultural uses is described in Section 3. In Section 4, we discuss the details of how to integrate the proposed approach into the treatment of sludge in sewage treatment plants. In Section 5, a mathematical model that, starting from the quantification of the ultrasonic power, provides a coupled differential model for the spatiotemporal reconstruction of temperature and humidity by also obtaining the pressure distribution inside the sewage tank is formulated. Once the sewage tank has been simulated using the FEM approach (Section 6) and a possible analytical model was proposed to evaluate the pressure exerted by the sludge on it (Section 7), the most important results for the analyses performed in both steady-state and transient regimes, as proposed in Section 8 have been discussed. Section 9 describes the prototype implemented for moisture detection and reduction in a sludge treatment tank, highlighting how sonication significantly improved the performance of the whole process to improve sludge quality (Section 10). Then, a quick roundup of comparisons with known cases in the literature (Section 11) further confirmed that the proposed approach is valid in software and hardware. In the last section, some reflections and possible future developments of the current research are given.

2. Preliminary Laboratory Study: Sonication on a Sample

To test whether the sonication produces sludge that can be used for agricultural purposes, in compliance with European standards EN 12766-1 and EN 12766-2 [54], at the

Calabria Service Laboratory we reproduced an ultrasonic bath using the instrumentation shown in Figure 1 capable of applying US waves with a constant frequency of 20 kHz (employing a platinum probe with a tip diameter of 25 mm, favoring cavitation since higher frequencies might not induce the phenomenon mentioned above), for 60 min (with a sampling time of 5 s) on four wastewater sludge samples of 125 mL each, placed in a 1-L beaker. In addition, the percentage of electric current generating the US wave of 20, 40, and 60% with power [W] values of 0.3, 0.8, and 1.6, respectively, were amplified, obtaining a temperature in degrees centigrade of 20, 28, and 36, respectively.

Figure 1. Test apparatus for the sludge pretreatment process by sonication.

During the process, selected parameters allow the transducer to convert electrical energy into mechanical waves, amplified by the booster, which is transmitted to the sludge, generate compression and rarefaction cycles, with the ultimate goal of reducing the sludge volume by at least 15–20%, resulting in a reduction of the maturation time by about 20–30% (reduction from 20 to 14 days) [54–56]. The effectiveness of sludge decomposition and solubilization was monitored by verifying the increase in chemical oxygen demand (COD) in the sludge substrate by titration using a burette, thermoreactor, and digestion vials [57].

ζ Potential and Polydispersity Index (PDI)

An important parameter for the characterization of sludge is represented by the ζ potential, which measures the electric charge on suspended particles. When it has a high absolute value (positive or negative), the particles repel each other, leading to a stable suspension. On the contrary, a low absolute value for it suggests that the particles can aggregate [58]. Furthermore, for the optimization of treatment processes, operators optimize the dosage of coagulants and flocculants by varying the ζ potential. This process ensures efficient particle aggregation and improves the overall efficiency of sludge dewatering and sedimentation processes [18]. To provide a detailed view of the causes of dispersion, aggregation, or flocculation, we measured the particle size of the sonified sludge (and thus the stability of the sludge). We measured the values of the ζ potential [mV], defined as $\frac{\eta u \eta}{\epsilon_0}$, the viscosity of the fluid; u the mobility; ϵ, relative dielectric constant; ϵ_0, permittivity of vacuum) representing the electrical potential at the level of the slipping plane (slipping plane) measuring the magnitude of electrostatic repulsion/attraction or charge between the particles during all the tests performed, showing good stability of the samples, since, for each of them, we obtained $\zeta \gg 40$ mV. PDI values, defined as the ratio of particle size σ^2 to the square of their diameter $\bar{d}^2$, were also evaluated, quantifying size dispersion (a value close to zero indicates a uniform distribution of particles, while a high value reflects a broader and less homogeneous distribution). Specifically, from the initial high values of PDI obtained (ranging between 15 and 20), following treatment, they were reduced between 0.921 ± 0.150 and 0.922 ± 0.150. Both ζ and PDI values were obtained through the Malvern Zetasizer. This instrument measures, with high accuracy, the size, charge, and concentration of particles (by dynamic light scattering (DLS) with a measurement angle of

90 degrees) and their molecular weight, as well as the amount of suspended molecules. The analysis was conducted at different temperatures and durations using appropriate cuvettes.

3. How the Proposed Procedure Enables the Production of Sludge for Agricultural Uses

The US technique tested in the Laboratory was integrated into an established sludge treatment process displayed in Figure 2 (whose steps are included in the red dashed box), while the proposed approach is highlighted with green hatching.

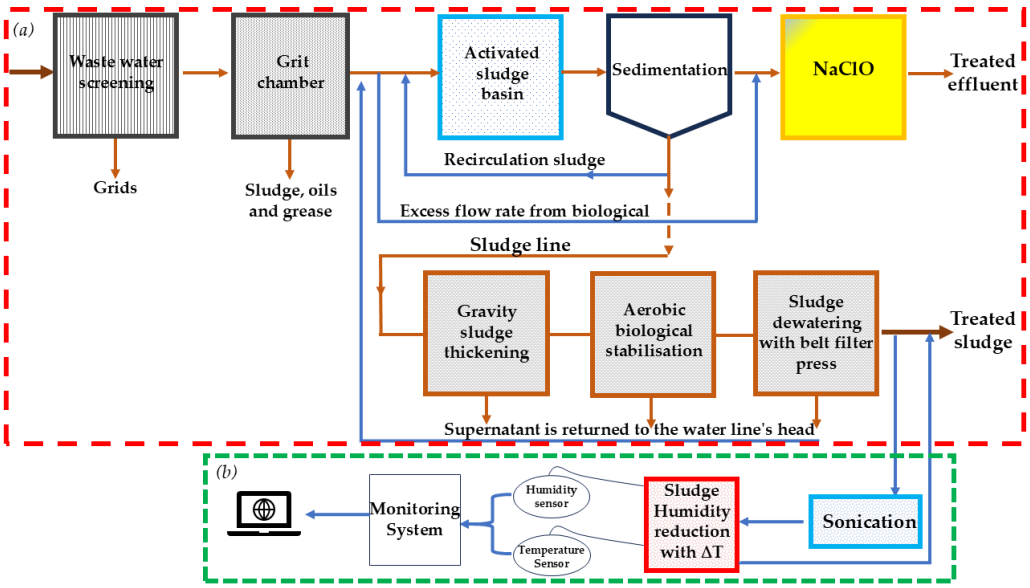

Figure 2. Integration of the proposed approach (enclosed by the green dashed line) into the sludge treatment process within a wastewater treatment plant (red dashed line). Section (**a**) represents the conventional wastewater treatment chain, including pretreatment, sedimentation, biological treatment, and sludge management. Section (**b**) highlights the proposed approach, combining monitoring by humidity and temperature sensors with a sonication system aimed at sludge moisture reduction (sludge humidity reduction with ΔT).

Sludge from wastewater undergoes a first treatment line (water line) that deals with the purification of the water to remove contaminants and return it to the environment following regulatory standards. In contrast, the sludge line manages the sludge produced from the water line processes, aiming to stabilize it, reduce its volume, and valorize it, for example, through biogas production. The water line treats the main water stream, while the sludge line focuses on solid by-product management, working in synergy as sludge comes from the former's processes, and the latter's residues can be recirculated for further treatment. Specifically, the water line processes sludge from wastewater that undergoes initial screening through a screening battery that separates heavy parts (coarse sands and gravels), allowing the filtered sludge to undergo treatment to remove fats and oils. Then, an aerobic digestion chamber facilitates prolonged aerobic treatment (of about 17–20 days) and proceeds with appropriate sedimentation. The fraction of sludge that is insufficiently oxygenated is fed back into the aerobic digestion chamber to repeat the process, while the remainder undergoes NaClO-based treatment to reduce the presence of pathogenic microorganisms, bacteria, viruses, and other contaminants, making the sludge safer for the environment [59]. It is worth noting that in excess flow rates from biological, once the oils and fats are removed, the sludge goes directly to NaClO-based treatment. A further portion of the sludge exiting sedimentation constitutes the input to the sludge line, which, through gravity sludge thickening, aerobic biological stabilization, and sludge dewatering

with belt filter press, produces the treated sludges (any supernatant is returned to the water line's head to be fed into the aerobic chamber). Then, before the treated sludge is considered waste (to produce dry sludge for agricultural use) at the end of the sludge line, the proposed procedure subjects it to the sonication process as already described so that the moisture percentage is significantly reduced by appropriate heat treatment. Finally, a monitoring system based essentially on moisture and temperature sensors sets the sonication parameters to optimize the whole process.

4. Integration of an Innovative Approach in the Treatment of Sludge in Sewage Treatment Plants

Laboratory-tested sonication treatment grafted inside the plant (see Figure 2) lasting up to 150 min, with the usual sampling carried out every 5 min (measuring COD, temperature, and PDI), was performed on an 8-liter sludge sample, applying a 230 V amplitude voltage at 50 Hz (constant frequency throughout the treatment duration), with a maximum flow rate of 50 L/min, with a contact time (total time the slurry remains in contact with a chemical reagent) per liter of 2.40 s. Four units with a peak power of 1.7 A were used to produce US waves to achieve the ideal US frequency of 150 kHz, corresponding to maximum cavitation. As can be seen from Table 2, the data obtained do not reveal any incompatibilities of sludge use for agricultural purposes, both in terms of heavy metals and the possible presence of bacteria (Salmonella). It is worth noting that both the treatment duration (150 min) and the contact time of 2.40 s depend on the sludge composition [60]. The prototype is powered by four sets of US generators, each with a maximum draw of 1.7 A to ensure the ideal frequency of 15 kHz, leading to the maximum detected cavitation (usually achievable between 1.5 A and 1.7 A). Table 3 summarizes the operational parameters of sonication, while the experimental apparatus is displayed in Figure 3.

Therefore, we consider proceeding with sludge humidity reduction using a thermal approach. We propose a physical–mathematical model that couples temperature with humidity to accurately quantify the volume of liquid and condensate inside the sludge treatment tank.

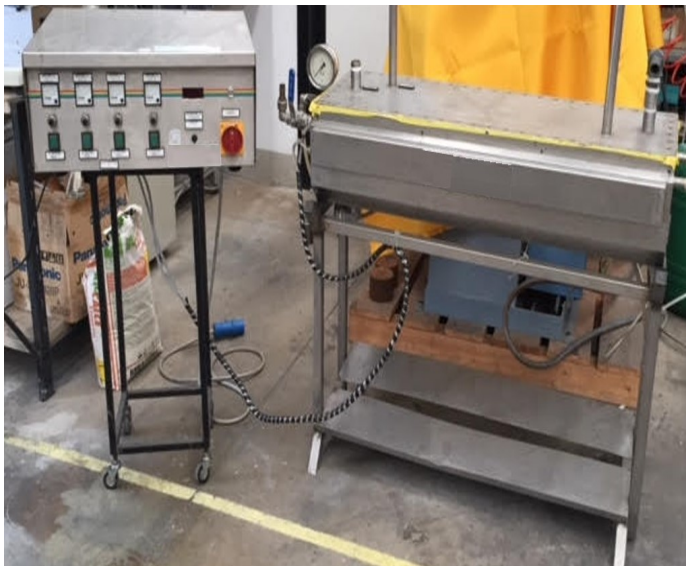

Figure 3. The experimental apparatus for sludge treatment process by ultrasonic sonication. **Left**: the amplifying device with current values increasing in percentage from 0 to 60 A. **Right**: the tank containing the sludge during ultrasonic sonication.

Table 2. Comparison between the parameters given in DL99 for sludge use in agriculture and the data collected on the sludge produced by the plant.

Heavy Metals (mg/kg) and Bacteria (MPN/gSS)	National Decree DL99—29 January 1992	Sludge Analysis of the Plant
arsenic	n.d.	//
copper	1000	700–800
zinc	2500	700–1200
cadmium	20	<1
mercury	10	<1
lead	750	90–160
nickel	300	50–90
organic carbon (% sludge)	20 (minimum)	25–30
phosphorus (% sludge)	20 (minimum)	25–30
nitrogen (% sludge)	1.5 (minimum)	4.5–5.5
salmonella	103 (maximum)	30–60

Table 3. Operating parameter of sludge sonication treatment.

Parameters	Values
Dimensions	445 × 545 × 1560 mm
Electrical supply	230 V, 50 Hz
US frequency	50 kHz, constant
Tank volume	8 L
Maximum input flow rate	3000 L/h, i.e., 50 L/min
Contact time	2.40 s per every sludge sample
Sonication time	0–150 min, sampling time 5 min

5. Temperature–Humidity Coupled Model for Sludge Treatment

5.1. Quantification of the Acoustic Power

Let $Oxyz$ be an ortho-normal Cartesian coordinate system where $\Omega \subset \mathbb{R}^3$ represents the sludge; then, the generic vector $\mathbf{x} = (x, y, z) \subset \Omega$ represents a point on the sludge. The acoustic energy, E, generated and transferred to the sludge sample during US sonication (following pretreatment in an oven at the initial temperature of 373 °C for two hours) is transformed, in part, into heat that produces an increase in temperature $T(\mathbf{x}, t)$ that can be quantified using a calorimetric approach (highlighting the direct proportionality between $T(\mathbf{x}, t)$ and P). The idea is based on the thermodynamic principle that P supplied by the US is converted into heat, and thus, the acoustic power can be calculated by measuring the temperature rise in the sludge.

The US energy (expressed in J) that causes an increase in $T(\mathbf{x}, t)$ can be expressed as [61–63]:

$$Q = MC_p \Delta T(\mathbf{x}, t) \tag{1}$$

where Q and M are the amount of heat absorbed by the slurry and its mass M (kg); C_p is the specific heat capacity (J/kg K); and $\Delta T(\mathbf{x}, t)$ is the increment of $T(\mathbf{x}, t)$ (K) (experimentally measurable by sensors). Then, the power P, if Δt is the time interval during which heat transfer occurred, takes the form:

$$P = \frac{MC_p \Delta T(\mathbf{x}, t)}{\Delta t}, \tag{2}$$

which, in an infinitesimal time frame, becomes:

$$P = MC_p \frac{dT(\mathbf{x}, t)}{dt}. \tag{3}$$

5.2. Fourier's Law of Heat Conduction

To quantify the heat flux, $\mathbf{q}$ (amount of heat per unit area in unit time measured in W/m^2), in the sludge as a function of $T(\mathbf{x}, t)$, we use the well-known Fourier's law:

$$\mathbf{q} = -k\nabla T(\mathbf{x}, t), \tag{4}$$

asserting that $\mathbf{q} \propto \nabla T(\mathbf{x}, t)$ through k (W/mK) representing the thermal conductivity of the sludge, with obvious heat flow from higher-temperature points to lower-temperature points.

5.3. General Thermal Balance Equation

A heat balance equation is essential to describe the thermal behavior in ultrasonic sludge treatment, considering heat transfer mechanisms and internal and external energy sources. This equation allows modeling the interactions between key variables and physical parameters, making it essential to simulate and optimize the process [61–63].

5.3.1. Thermal Storage Term

Together with C_p, it describes the ability of the fluid to store thermal energy. $\frac{\partial T(\mathbf{x},t)}{\partial t}$ measures the rate at which $T(\mathbf{x}, t)$ changes over time. Therefore, the contribution due to accumulation can be quantified by the term $\rho C_p \frac{\partial T(\mathbf{x},t)}{\partial t}$. The contribution due to heat accumulation in the sludge can be quantified as $\rho C_p \frac{\partial T(\mathbf{x},t)}{\partial t}$ where ρ is the density of the fluid while C_p denotes the capacity of the sludge to store heat [61–63].

5.3.2. Convective Term

This term represents heat transport by convection, describing how the motion of a slurry at the velocity $\mathbf{u}(\mathbf{x}, t)$ transports heat energy, influencing the energy balance with the contribution $\rho C_p \mathbf{u}(\mathbf{x}, t) \cdot \nabla T(\mathbf{x}, t)$, which quantifies the heat gain or loss in the system [61–63].

5.3.3. Heat Conduction Term

This term represents heat flow by conduction and quantifies how it varies spatially, indicating whether heat enters or leaves a specific region of the fluid, expressed as $\nabla \cdot (-k\nabla T(\mathbf{x}, t))$ based on the temperature gradient [61–63].

5.3.4. Heat Sources

Denoted by $Q(\mathbf{x}, t)$ and $Q_m(\mathbf{x}, t)$, respectively, they represent heat added by an external source (e.g., an external heater) and heat generated inside the system due to internal causes (e.g., chemical reactions or biological processes). Then, the heat generated in the US can act directly by converting P to heat within the sludge; the second allows the mechanical energy generated by the US to break up the particles, facilitating heat diffusion and accelerating the process of temperature homogenization [61–63].

5.4. The Energy Balance Equation

Combining all the contributions, we obtain:

$$\begin{aligned} \rho C_p \tfrac{\partial T(\mathbf{x},t)}{\partial t} + \rho C_p \mathbf{u}(\mathbf{x}, t) \cdot \nabla T(\mathbf{x}, t) + \nabla \cdot (-k\nabla T(\mathbf{x}, t)) = \\ = Q(\mathbf{x}, t) + Q_m(\mathbf{x}, t). \end{aligned} \tag{5}$$

representing the parabolic differential equation of the second-order partial derivative that governs the energy balance by describing the evolution of $T(\mathbf{x}, t)$, which considers all modes of energy transfer (conduction, convection, internal and/or external heat sources). The model

(5) describes the heat transfer and the variation of $T(\mathbf{x}, t)$ in the system, influenced directly by P. Heat conduction depends on the energy transferred per unit time and area, a function of P, while ultrasonic convection and turbulence influence heat transport in the fluid. Therefore, the acoustic power determines the thermal behavior of the model [61–65].

5.5. On Moisture Reduction

To calculate the reduction of moisture $W(\mathbf{x}, t)$ in a sludge from $T(\mathbf{x}, t)$, we use a model based on the Balance Equation (5). $W(\mathbf{x}, t)$, representing the water content per unit volume, varies with the evaporative flux, $J_e(\mathbf{x}, t)$, described as:

$$\frac{\partial W(\mathbf{x}, t)}{\partial t} = -\nabla \cdot J_e(\mathbf{x}, t), \tag{6}$$

where $J_e(J_e(\mathbf{x}, t)$ is a function of $T(\mathbf{x}, t)$ and vapor pressure, and is written as:

$$J_e(\mathbf{x}, t) = k_e(T(\mathbf{x}, t))\big(p_v(T(\mathbf{x}, t)) - p_{v,\text{amb}}\big), \tag{7}$$

with $k_e(T(\mathbf{x}, t))$ temperature-dependent evaporation coefficient, $p_v(T(\mathbf{x}, t))$ saturated vapor pressure and $p_{v,\text{amb}}$ ambient vapor pressure. The source $Q_m(\mathbf{x}, t)$, associated with water evaporation, is related to the latent heat λ and the rate of moisture reduction:

$$Q_m(\mathbf{x}, t) = \lambda \frac{\partial W(\mathbf{x}, t)}{\partial t}. \tag{8}$$

The overall moisture reduction is calculated by integrating the residual content $W(\mathbf{x}, t)$ over time and space, compared with the initial content $W_0(\mathbf{x})$:

$$\Delta W = \int_\Omega \big(W_0(\mathbf{x}) - W(\mathbf{x}, t)\big)\, d\mathbf{x}. \tag{9}$$

Then, substituting into the (5) the (8), we obtain:

$$\begin{aligned} \rho C_p \frac{\partial T(\mathbf{x}, t)}{\partial t} + \rho C_p \mathbf{u}(\mathbf{x}, t) \cdot \nabla T(\mathbf{x}, t) + \nabla \cdot (-k \nabla T(\mathbf{x}, t)) = \\ = Q(\mathbf{x}, t) + \lambda \frac{\partial W(\mathbf{x}, t)}{\partial t}. \end{aligned} \tag{10}$$

5.6. The Coupled System

Considering the balance equation, Equations (6) and (10), the system describing the evolution of temperature and humidity consists of:

$$\begin{cases} \rho C_p \frac{\partial T}{\partial t} + \rho C_p \mathbf{u} \cdot \nabla T + \nabla \cdot (-k \nabla T) = Q + \lambda \frac{\partial W(\mathbf{x}, t)}{\partial t}, \\ \frac{\partial W(\mathbf{x}, t)}{\partial t} + \nabla \cdot J_e(\mathbf{x}, t) = 0 \\ J_e(\mathbf{x}, t) = k_e(T(\mathbf{x}, t))\big(p_v(T(\mathbf{x}, t)) - p_{v,\text{amb}}\big). \end{cases} \tag{11}$$

5.7. On the Existence, Uniqueness, and Regularity of the Solution: Variational Formulation

We work on $\Omega \subset \mathbb{R}^n$, which is open, restricted, and with edge $\partial\Omega$ sufficiently regular. We define the Cartesian product of function spaces to describe the two coupled variables $T(\mathbf{x}, t)$ and $W(\mathbf{x}, t)$ [61–63,66]:

$$X = H^1(\Omega) \times H^1(\Omega), \tag{12}$$

where $H^1(\Omega)$ is the Sobolev space of functions belonging to $L^2(\Omega)$ with first-order weak derivatives in $L^2(\Omega)$. Weak solutions of the coupled system will be looked for

in $\mathcal{X} = L^2(0, T; X)$, with time derivatives $\frac{\partial T(\mathbf{x},t)}{\partial t}, \frac{\partial W(\mathbf{x},t)}{\partial t} \in L^2(0, T; X')$, where X' is the dual space of X'. We multiply the budget equation in (11) by a test function $\varphi \in H^1(\Omega)$ and integrate over Ω, obtaining:

$$\int_\Omega \rho C_p \frac{\partial T(\mathbf{x},t)}{\partial t} \varphi \, d\mathbf{x} + \int_\Omega \rho C_p (\mathbf{u} \cdot \nabla T) \varphi \, d\mathbf{x} + \int_\Omega k \nabla T(\mathbf{x},t) \cdot \nabla \varphi \, d\mathbf{x} = \\ = \int_\Omega Q \varphi \, d\mathbf{x} + \lambda \int_\Omega \frac{\partial W(\mathbf{x},t)}{\partial t} \varphi \, d\mathbf{x}. \tag{13}$$

To ensure that the first integral in (13) makes sense, we assume $T(\mathbf{x},t) \in L^2(0, T; H^1(\Omega))$ and $\frac{\partial T(\mathbf{x},t)}{\partial t} \in L^2(0, T; H^1(\Omega)')$. As for the second equation in (11), we multiply by a test function $\psi \in H^1(\Omega)$ and integrate over Ω, obtaining:

$$\int_\Omega \frac{\partial W(\mathbf{x},t)}{\partial t} \psi \, d\mathbf{x} + \int_\Omega (\nabla \cdot J_e) \psi \, d\mathbf{x} = 0. \tag{14}$$

Using, then, the divergence theorem and imposing a natural boundary condition ($J_e \cdot \mathbf{n} = 0$ on $\partial\Omega$), we can write:

$$\int_\Omega (\nabla \cdot J_e) \psi \, d\mathbf{x} = - \int_\Omega J_e \cdot \nabla \psi \, d\mathbf{x}. \tag{15}$$

Then the second equation of (11) in variational form becomes:

$$\int_\Omega \frac{\partial W(\mathbf{x},t)}{\partial t} \psi \, d\mathbf{x} - \int_\Omega J_e \cdot \nabla \psi \, d\mathbf{x} = 0, \tag{16}$$

that by substituting into it the expression of J_e, we obtain:

$$\int_\Omega \frac{\partial W(\mathbf{x},t)}{\partial t} \psi \, d\mathbf{x} - \int_\Omega k_e(T) \big(p_v(T) - p_{v,\text{amb}}\big) \nabla \psi \, d\mathbf{x} = 0. \tag{17}$$

Then, the problem, in weak form, translates to finding a solution $(T(\mathbf{x},t), W(\mathbf{x},t)) \in L^2(0, T; X)$, such that for each test function $(\varphi, \psi) \in X$ both equations in the variational form are satisfied.

5.7.1. Existence and Uniqueness

We define the paired bilinear operator $\mathcal{A} : X \times X \to \mathbb{R}$ as [61–63]:

$$\mathcal{A}((T(\mathbf{x},t), W(\mathbf{x},t)), (\varphi, \psi)) = \\ = \int_\Omega k \nabla T(\mathbf{x},t) \cdot \nabla \varphi \, d\mathbf{x} + \int_\Omega \rho C_p (\mathbf{u} \cdot \nabla T(\mathbf{x},t)) \varphi \, d\mathbf{x} + \\ + \int_\Omega k_e(T) \big(p_v(T) - p_{v,\text{amb}}\big) \nabla \psi \, d\mathbf{x}. \tag{18}$$

It is simple to verify that the operator $\mathcal{A}$ is continuous, i.e., there exists $C > 0$ such that:

$$|\mathcal{A}((T(\mathbf{x},t), W(\mathbf{x},t)), (\varphi, \psi))| \leq \\ \leq C(\|T(\mathbf{x},t)\|_{H^1} + \|W(\mathbf{x},t)\|_{H^1})(\|\varphi\|_{H^1} + \|\psi\|_{H^1}). \tag{19}$$

Moreover, $\mathcal{A}$ is coercive under the assumptions of uniform positivity of the coefficients ($k(x) \geq k_0 > 0$):

$$\begin{aligned}\mathcal{A}((T(\mathbf{x},t),W(\mathbf{x},t)),(T(\mathbf{x},t),W(\mathbf{x},t))) \geq \\ \geq \alpha(\|T(\mathbf{x},t)\|^2_{H^1} + \|W(\mathbf{x},t)\|^2_{H^1}),\end{aligned} \tag{20}$$

where $\alpha > 0$. The functional associated with the source and coupling terms is:

$$F((\varphi,\psi)) = \int_\Omega Q\varphi \, d\mathbf{x} + \lambda \int_\Omega \frac{\partial W}{\partial t}\varphi \, d\mathbf{x} + \int_\Omega \frac{\partial W}{\partial t}\psi \, d\mathbf{x}. \tag{21}$$

Under the assumptions of regularity ($Q \in L^2(\Omega)$, $\frac{\partial W}{\partial t} \in L^2(0,T;H^1(\Omega)')$, F is continuous. Then, the Lax-Milgram theorem guarantees the existence and uniqueness of $(T,W) \in L^2(0,T;X)$.

5.7.2. Regularity

The regularity of the solutions $T(\mathbf{x},t)$ and $W(\mathbf{x},t)$ can be analyzed by exploiting the coupled structure of the system. In particular, the time derivative $\dfrac{\partial T(\mathbf{x},t)}{\partial t}$ belongs to $L^2(0,T;H^1(\Omega)')$. This result is ensured by the regularity of $W(\mathbf{x},t)$, which belongs to $L^2(0,T;H^1(\Omega))$, and by the fact that the coupling term $\lambda\frac{\partial W(\mathbf{x},t)}{\partial t}$ is sufficiently regular. Consequently, $T(\mathbf{x},t)$ evolves in time regularly within a weak functional space.

The elliptic structure of the term $-\nabla\cdot(k\nabla T(\mathbf{x},t))$ in the first equation also guarantees that $T(\mathbf{x},t) \in H^1(\Omega)$ at each instant t, provided that k, $\mathbf{u}$, Q are regular. If k is sufficiently regular, e.g., $k \in C^2(\Omega)$, we can conclude that $T(\mathbf{x},t) \in H^2(\Omega)$ for each instant t.

The regularity of the solution $W(\mathbf{x},t)$ depends directly on the regularity of $T(\mathbf{x},t)$ through the nonlinear term $J_e = k_e(T)\big(p_v(T) - p_{v,\text{amb}}big\big)$. If $T(T(\mathbf{x},t) \in H^1(\Omega)$, then $W(\mathbf{x},t) \in H^1(\Omega)$. If moreover $T(\mathbf{x},t) \in H^2(\Omega)$ and the coefficients $k_e(T)$ and $p_v(T)$ are regular, e.g., C^2, then we can conclude that W also belongs to $H^2(\Omega)$.

6. The Numerical Model

6.1. Time Discretization

We apply the implicit Euler's method for the temporal discretization of the terms $\frac{\partial T}{\partial t}$ and $\frac{\partial W}{\partial t}$, obtaining: [61–63]

$$\frac{\partial T}{\partial t} \approx \frac{T^{n+1}-T^n}{\Delta t}, \quad \frac{\partial W}{\partial t} \approx \frac{W^{n+1}-W^n}{\Delta t}, \tag{22}$$

which substituted in the variational formulation, gives, for T^{n+1}:

$$\begin{aligned}\int_\Omega \rho C_p \frac{T^{n+1}-T^n}{\Delta t}\varphi \, d\mathbf{x} + \int_\Omega \rho C_p(\mathbf{u}\cdot\nabla T^{n+1})\varphi \, d\mathbf{x} + \int_\Omega k\nabla T^{n+1}\cdot\nabla\varphi \, d\mathbf{x} = \\ = \int_\Omega Q\varphi \, d\mathbf{x} + \lambda\int_\Omega \frac{W^{n+1}-W^n}{\Delta t}\varphi \, d\mathbf{x},\end{aligned} \tag{23}$$

and for W^{n+1}:

$$\int_\Omega \frac{W^{n+1}-W^n}{\Delta t}\psi \, d\mathbf{x} - \int_\Omega k_e(T^{n+1})\big(p_v(T^{n+1}) - p_{v,\text{amb}}\big)\nabla\psi \, d\mathbf{x} = 0. \tag{24}$$

As for spatial discretization, we partition Ω into a mesh $\mathcal{T}_h$, composed of M finite elements. We approximate the solutions T^{n+1} and W^{n+1} as linear combinations of basis functions $\phi_i(\mathbf{x})$, as follows:

$$T_h^{n+1}(\mathbf{x}) = \sum_{i=1}^{N} T_i^{n+1}\phi_i(\mathbf{x}), \quad W_h^{n+1}(\mathbf{x}) = \sum_{i=1}^{N} W_i^{n+1}\phi_i(\mathbf{x}), \tag{25}$$

where T_i^{n+1} and W_i^{n+1} are the values of the solutions at the nodes of the mesh. The test functions are chosen from the same basis, namely $\varphi = \phi_i$ and $\psi = \phi_j$.
Then, substituting these expansions into the variational equations, we obtain for T^{n+1}:

$$\begin{aligned} &\sum_{j=1}^{N}\left[\int_\Omega \rho C_p \frac{\phi_j\phi_i}{\Delta t}\,d\mathbf{x}\right]T_j^{n+1} + \\ &+\sum_{j=1}^{N}\left[\int_\Omega k\nabla\phi_j\cdot\nabla\phi_i\,d\mathbf{x} + \int_\Omega \rho C_p(\mathbf{u}\cdot\nabla\phi_j)\phi_i\,d\mathbf{x}\right]T_j^{n+1} = \\ &= \int_\Omega Q\phi_i\,d\mathbf{x} + \sum_{j=1}^{N}\left[\int_\Omega \frac{\lambda\phi_j\phi_i}{\Delta t}\,d\mathbf{x}\right]W_j^{n+1} - \int_\Omega \frac{\rho C_p T^n\phi_i}{\Delta t}\,d\mathbf{x}, \end{aligned} \tag{26}$$

and for W^{n+1}:

$$\begin{aligned} &\sum_{j=1}^{N}\left[\int_\Omega \frac{\phi_j\phi_i}{\Delta t}\,d\mathbf{x}\right]W_j^{n+1} - \\ &-\sum_{j=1}^{N}\left[\int_\Omega k_e(T^{n+1})\big(p_v(T^{n+1}) - p_{v,\mathrm{amb}}\big)\nabla\phi_j\cdot\nabla\phi_i\,d\mathbf{x}\right]W_j^{n+1} = \int_\Omega \frac{\phi_i W^n}{\Delta t}\,d\mathbf{x}. \end{aligned} \tag{27}$$

6.2. Algebraic Formulation

For computational needs, we define the mass matrix and stiffness matrix for T as:

$$(\mathbf{M}_T)_{ij} = \int_\Omega \rho C_p\phi_j\phi_i\,d\mathbf{x}. \tag{28}$$

and:

$$(\mathbf{A}_T)_{ij} = \int_\Omega k\nabla\phi_j\cdot\nabla\phi_i\,d\mathbf{x} + \int_\Omega \rho C_p(\mathbf{u}\cdot\nabla\phi_j)\phi_i\,d\mathbf{x}. \tag{29}$$

respectively, while, for W, the mass and stiffness matrix (dependent on T), take the following forms:

$$(\mathbf{M}_W)_{ij} = \int_\Omega \phi_j\phi_i\,d\mathbf{x}, \tag{30}$$

$$(\mathbf{A}_W(T))_{ij} = \int_\Omega k_e(T)\big(p_v(T) - p_{v,\mathrm{amb}}\big)\nabla\phi_j\cdot\nabla\phi_i\,d\mathbf{x}. \tag{31}$$

Finally, considering the source term:

$$(\mathbf{F}_T)_i = \int_\Omega Q\phi_i\,d\mathbf{x}, \quad (\mathbf{F}_W)_i = \int_\Omega \phi_i W^n\,d\mathbf{x}, \tag{32}$$

our coupled linear system becomes:

$$\begin{cases} \mathbf{M}_T\frac{\mathbf{T}^{n+1}-\mathbf{T}^n}{\Delta t} + \mathbf{A}_T\mathbf{T}^{n+1} = \mathbf{F}_T + \lambda\mathbf{M}_T\frac{\mathbf{W}^{n+1}-\mathbf{W}^n}{\Delta t} \\ \mathbf{M}_W\frac{\mathbf{W}^{n+1}-\mathbf{W}^n}{\Delta t} - \mathbf{A}_W(\mathbf{T}^{n+1})\mathbf{W}^{n+1} = 0. \end{cases} \tag{33}$$

The resolution of the described coupled algebraic system requires numerical methods since it includes nonlinear dependencies and couplings between the variables $\mathbf{T}^{n+1}$ and $\mathbf{W}^{n+1}$. The system (33) can be written in the following form:

$$\begin{bmatrix} \mathbf{M}_T/\Delta t + \mathbf{A}_T & -\lambda \mathbf{M}_T/\Delta t \\ 0 & \mathbf{M}_W/\Delta t - \mathbf{A}_W(\mathbf{T}^{n+1}) \end{bmatrix} \begin{bmatrix} \mathbf{T}^{n+1} \\ \mathbf{W}^{n+1} \end{bmatrix} = \\ = \begin{bmatrix} \mathbf{F}_T + \mathbf{M}_T\mathbf{T}^n/\Delta t + \lambda \mathbf{M}_T\mathbf{W}^n/\Delta t \\ \mathbf{M}_W\mathbf{W}^n/\Delta t \end{bmatrix}. \tag{34}$$

It is nonlinear, since $\mathbf{A}_W(\mathbf{T}^{n+1})$ depends on $\mathbf{T}^{n+1}$). Then, using an iterative approach based on Newton-Raphson, we define the residual as:

$$\mathbf{R}(\mathbf{T}, \mathbf{W}) = \begin{bmatrix} \mathbf{M}_T \frac{\mathbf{T}-\mathbf{T}^n}{\Delta t} + \mathbf{A}_T\mathbf{T} - \lambda \mathbf{M}_T \frac{\mathbf{W}-\mathbf{W}^n}{\Delta t} - \mathbf{F}_T \\ \mathbf{M}_W \frac{\mathbf{W}-\mathbf{W}^n}{\Delta t} - \mathbf{A}_W(\mathbf{T})\mathbf{W} \end{bmatrix}, \tag{35}$$

such that we find $(\mathbf{T}^{n+1}, \mathbf{W}^{n+1})$ such that $\mathbf{R}(\mathbf{T}^{n+1}, \mathbf{W}^{n+1}) = 0$. Then, we expand $\mathbf{R}(\mathbf{T}, \mathbf{W})$ around an initial estimate $(\mathbf{T}_k, \mathbf{W}_k)$ at step k using a Taylor series:

$$\mathbf{R}(\mathbf{T}_{k+1}, \mathbf{W}_{k+1}) \approx \mathbf{R}(\mathbf{T}_k, \mathbf{W}_k) + \frac{\partial \mathbf{R}}{\partial \mathbf{T}}\Delta\mathbf{T} + \frac{\partial \mathbf{R}}{\partial \mathbf{W}}\Delta\mathbf{W}, \tag{36}$$

where:

$$\Delta\mathbf{T} = \mathbf{T}_{k+1} - \mathbf{T}_k, \quad \Delta\mathbf{W} = \mathbf{W}_{k+1} - \mathbf{W}_k. \tag{37}$$

6.3. Linearization of the Algebraic System

Linearizing the coupled system, we obtain the following linear system:

$$\begin{bmatrix} \frac{\partial \mathbf{R}_T}{\partial \mathbf{T}} & \frac{\partial \mathbf{R}_T}{\partial \mathbf{W}} \\ \frac{\partial \mathbf{R}_W}{\partial \mathbf{T}} & \frac{\partial \mathbf{R}_W}{\partial \mathbf{W}} \end{bmatrix} \begin{bmatrix} \Delta\mathbf{T} \\ \Delta\mathbf{W} \end{bmatrix} = -\begin{bmatrix} \mathbf{R}_T(\mathbf{T}_k, \mathbf{W}_k) \\ \mathbf{R}_W(\mathbf{T}_k, \mathbf{W}_k) \end{bmatrix}, \tag{38}$$

where:

$$\frac{\partial \mathbf{R}_T}{\partial \mathbf{T}} = \frac{\mathbf{M}_T}{\Delta t} + \mathbf{A}_T, \quad \frac{\partial \mathbf{R}_T}{\partial \mathbf{W}} = -\frac{\lambda \mathbf{M}_T}{\Delta t}, \tag{39}$$

$$\frac{\partial \mathbf{R}_W}{\partial \mathbf{T}} = -\frac{\partial \mathbf{A}_W(\mathbf{T})}{\partial \mathbf{T}}\mathbf{W}, \quad \frac{\partial \mathbf{R}_W}{\partial \mathbf{W}} = \frac{\mathbf{M}_W}{\Delta t} - \mathbf{A}_W(\mathbf{T}) \tag{40}$$

where $\frac{\partial \mathbf{A}_W(\mathbf{T})}{\partial \mathbf{T}}$ is a matrix that is calculated by differentiating $\mathbf{A}_W(\mathbf{T})$ with respect to $\mathbf{T}$. At each iteration, k the system becomes [61–63]:

$$\begin{bmatrix} \frac{\mathbf{M}_T}{\Delta t} + \mathbf{A}_T & -\frac{\lambda \mathbf{M}_T}{\Delta t} \\ -\frac{\partial \mathbf{A}_W(\mathbf{T}_k)}{\partial \mathbf{T}}\mathbf{W}_k & \frac{\mathbf{M}_W}{\Delta t} - \mathbf{A}_W(\mathbf{T}_k) \end{bmatrix} \begin{bmatrix} \Delta\mathbf{T} \\ \Delta\mathbf{W} \end{bmatrix} = -\begin{bmatrix} \mathbf{R}_T(\mathbf{T}_k, \mathbf{W}_k) \\ \mathbf{R}_W(\mathbf{T}_k, \mathbf{W}_k) \end{bmatrix}. \tag{41}$$

from which the updating of solutions is ensured as follows:

$$\mathbf{T}_{k+1} = \mathbf{T}_k + \Delta\mathbf{T}, \quad \mathbf{W}_{k+1} = \mathbf{W}_k + \Delta\mathbf{W}. \tag{42}$$

Obviously, iterations proceed to that some residual, $\epsilon < 0$, satisfies:

$$\|\mathbf{R}_T(\mathbf{T}_{k+1}, \mathbf{W}_{k+1})\| + \|\mathbf{R}_W(\mathbf{T}_{k+1}, \mathbf{W}_{k+1})\| < \epsilon. \tag{43}$$

Then, calculating the matrices $\mathbf{M}_T$, $\mathbf{M}_W$, $\mathbf{A}_T$, and the basic form of $\mathbf{A}_W(\mathbf{T})$, for each time step $n+1$, we initialize $\mathbf{T}_0^{n+1} = \mathbf{T}^n$ and $\mathbf{W}_0^{n+1} = \mathbf{W}^n$ and perform Newton-Raphson iterations until convergence. The solution $(\mathbf{T}^{n+1}, \mathbf{W}^{n+1})$ gives the updated values of the variables at the next time step.

Solution of the Algebraic System

At each iteration, the linear system can be written in the following form:

$$\mathbf{K}\begin{bmatrix}\Delta\mathbf{T}\\ \Delta\mathbf{W}\end{bmatrix} = -\begin{bmatrix}\mathbf{R}_T(\mathbf{T}_k,\mathbf{W}_k)\\ \mathbf{R}_W(\mathbf{T}_k,\mathbf{W}_k)\end{bmatrix}, \tag{44}$$

where:

$$\mathbf{K} = \begin{bmatrix}\mathbf{K}_{TT} & \mathbf{K}_{TW}\\ \mathbf{K}_{WT} & \mathbf{K}_{WW}\end{bmatrix}, \tag{45}$$

with:

$$\mathbf{K}_{TT} = \frac{\mathbf{M}_T}{\Delta t} + \mathbf{A}_T, \quad \mathbf{K}_{TW} = -\frac{\lambda\mathbf{M}_T}{\Delta t}, \tag{46}$$

$$\mathbf{K}_{WT} = -\frac{\partial\mathbf{A}_W(\mathbf{T}_k)}{\partial\mathbf{T}}\mathbf{W}_k, \quad \mathbf{K}_{WW} = \frac{\mathbf{M}_W}{\Delta t} - \mathbf{A}_W(\mathbf{T}_k). \tag{47}$$

Whose known term is:

$$\mathbf{b} = -\begin{bmatrix}\mathbf{R}_T(\mathbf{T}_k,\mathbf{W}_k)\\ \mathbf{R}_W(\mathbf{T}_k,\mathbf{W}_k)\end{bmatrix}. \tag{48}$$

Once the matrices $\mathbf{M}_T$, $\mathbf{M}_W$, $\mathbf{A}_T$, $\mathbf{A}_W(\mathbf{T}_k)$ are constructed by FEM discretization, $\mathbf{K}$ is constructed as a sparse block matrix in which $\mathbf{K}_{TT}$ and $\mathbf{K}_{WW}$ are dominant diagonal matrices. Finally, the paired $\mathbf{K}_{TW}$ and $\mathbf{K}_{WT}$ blocks (calculated from the problem under study). Since the linear system is large with sparse matrices, GMRES is employed. For more complex problems, we can introduce a preconditioner based on the diagonal blocks $\mathbf{K}_{TT}$ and $\mathbf{K}_{WW}$ to speed up convergence.

6.4. Relationship Between $W(\mathbf{x},t)$ and the Liquid Water Content

To quantify the volume of liquid and condensate inside the sludge treatment tank, starting from temperature $T(\mathbf{x},t)$ and moisture $W(\mathbf{x},t)$, it is necessary to implement an approach that integrates the following steps. Since $W(\mathbf{x},t)$ represents the moisture content per unit volume of the sludge, to obtain the total volume of initial and residual liquid water in the tank, it will be sufficient to calculate:

$$V_{\text{water}}^{\text{inizial}} = \int_\Omega W_0(\mathbf{x})\,d\mathbf{x}, \quad V_{\text{water}}^{\text{residue}}(t) = \int_\Omega W(\mathbf{x},t)\,d\mathbf{x}, \tag{49}$$

where $W_0(W_0(\mathbf{x})$ is the initial moisture content. During heat treatment, some evaporated water condenses on the inner surfaces of the tank or accumulates as droplets. The volume of condensate can be quantified by balancing the evaporative flux and considering the fraction that turns into condensate. Then, from $J_e(\mathbf{x},t)$, the total evaporated water flux is calculated:

$$\dot{V}_{\text{evaporate}}(t) = \int_\Omega J_e(\mathbf{x},t)\,d\mathbf{x}. \tag{50}$$

Assuming that a fraction $\eta_t extcondensate$ of the evaporated volume turns into condensate (depending on environmental and system conditions), the total volume of condensate is given by:

$$V_{\text{condensate}}(t) = \int_0^t \eta_{\text{condensate}} \cdot \dot{V}_{\text{evaporate}}(\tau)\,d\tau. \tag{51}$$

The coefficient $\eta_t extcondensate$ can be determined experimentally or modeled from the pressure and temperature inside the tank. The total volume of liquid inside the tank, $V_{\text{liquid}}(t)$, includes the residual liquid in the sludge and the accumulated condensate:

$$V_{\text{liquid}}(t) = V_{\text{water}}^{\text{residue}}(t) + V_{\text{condensate}}(t). \tag{52}$$

Integrating the above terms on Ω yields, at each time step, $V_{\text{water}}^{\text{residue}}(t)$, $\dot{V}_{\text{evaporate}}(t)$, and $V_{\text{condensate}}(t)$, Obviously, it is essential to specify the flow and temperature conditions at the surface of the tank to model evaporation and condensation correctly.

6.5. FEM Calculations

To implement the FEM calculation of the volume of liquid and condensate in the tank, since $T(\mathbf{x}, t)$ and $W(\mathbf{x}, t)$ have already been obtained, we proceed as follows. Since the initial and residual volumes of water are calculated by integrating $W_0(\mathbf{x})$ and $W(\mathbf{x}, t)$ on the domain Ω, we can proceed with the following discretization:

$$V_{\text{water}}^{\text{inizial}} \approx \sum_{e=1}^{M} \int_{\Omega_e} W_0^h(\mathbf{x})\, d\mathbf{x}, \quad V_{\text{water}}^{\text{residue}}(t) \approx \sum_{e=1}^{M} \int_{\Omega_e} W^h(\mathbf{x}, t)\, d\mathbf{x}, \tag{53}$$

in which $W^h(\mathbf{x}, t) = \sum_{i=1}^{N} W_i(t)\phi_i(\mathbf{x})$ is the FEM approximation of $\mathbf{x}, t)$, while $\mathbf{x}(\mathbf{x})$ is the shape functions defined on the mesh. For each element of the mesh, Ω_e, we calculate:

$$\int_{\Omega_e} W^h(\mathbf{x}, t)\, d\mathbf{x} \approx \mathbf{W}_e^T \mathbf{M}_e, \tag{54}$$

where $\mathbf{M}_e$ represents the elemental mass matrix, whose generic element is given by:

$$(\mathbf{M}_e)_{ij} = \int_{\Omega_e} \phi_i \phi_j\, d\mathbf{x}. \tag{55}$$

Finally, adding up all the contributions, we will obtain:

$$V_{\text{water}}^{\text{residue}}(t) \approx \sum_{e=1}^{M} \mathbf{W}_e^T \mathbf{M}_e. \tag{56}$$

As for the evaporative flux given by (50), it can be approximated by:

$$\dot{V}_{\text{evaporate}}(t) = \int_{\Omega} J_e^h(\mathbf{x}, t)\, d\mathbf{x}, \tag{57}$$

where $J_e^h(\mathbf{x}, t)$ is the FEM approximation of the evaporative flux:

$$J_e^h(\mathbf{x}, t) = \sum_{i=1}^{N} J_{e,i}(t)\phi_i(\mathbf{x}). \tag{58}$$

Then, for each element Ω_e, we calculate

$$\int_{\Omega_e} J_e^h(\mathbf{x}, t)\, d\mathbf{x} \approx \mathbf{J}_e^T \mathbf{M}_e, \tag{59}$$

where $\mathbf{J}_e$ is the vector of nodal values of J_e on the element. Then, summing the contributions of all the elements, we have:

$$\dot{V}_{\text{evaporate}}(t) \approx \sum_{e=1}^{M} \mathbf{J}_e^T \mathbf{M}_e. \tag{60}$$

To compute the total volume of condensate (51) at each time step, we use the trapezoidal integration method:

$$V_{\text{condensate}}^{n+1} \approx V_{\text{condensate}}^{n} + \frac{\Delta t}{2} \cdot \eta_{\text{condensate}} \cdot \left(\dot{V}_{\text{evaporate}}^{n} + \dot{V}_{\text{evaporate}}^{n+1}\right), \tag{61}$$

where $\dot{V}^{n}_{\text{evaporated}}$ and $\dot{V}^{n+1}_{\text{evaporated}}$ are the evaporative fluxes at the time steps n and $n+1$, respectively, thus providing the total volume in the tank.

7. On the Pressure Exerted by the Sludge on the Tank

If $p(\mathbf{x}, t)$ represents the pressure exerted by the sludge on the tank, being coupled with both $T(\mathbf{x}, t)$ and $W(\mathbf{x}, t)$, its computation requires considering both thermodynamic and mechanical effects of the system. We preliminarily observe that $p(\mathbf{x}, t)$ is generally related to the thermodynamic behavior of the material and depends on the density of the slurry, $\rho(\mathbf{x}, t)$, compressibility $K(T, W)$, as well as $T(\mathbf{x}, t)$ and $W(\mathbf{x}, t)$. Without detracting in generality, we model $p(\mathbf{x}, t)$ by an equation of state describing the behavior of the material:

$$p(\mathbf{x}, t) = p_0 + K(T(\mathbf{x}, t), W(\mathbf{x}, t))[\rho(\mathbf{x}, t) - \rho_0], \tag{62}$$

where p_0 is the reference pressure (referenced to T_0, W_0), ρ_0 is the density of the sludge at T_0 and W_0, $K(T(\mathbf{x}, t), W(\mathbf{x}, t))$ is the compressibility modulus of the sludge. It is worth noting that $\rho(\mathbf{x}, t)$ varies as a function of $T(\mathbf{x}, t)$ and $W(\mathbf{x}, t)$ due to thermal expansion and change in water content, which, to a good approximation, leads to the following formulation:

$$\rho(\mathbf{x}, t) = \rho_0[1 - \beta_T(T(\mathbf{x}, t) - T_0) + \beta_W(W(\mathbf{x}, t) - W_0)], \tag{63}$$

where β_T is the coefficient of thermal expansion and β_W is the coefficient of change in density with respect to moisture. Similarly, for the compressibility of sludge:

$$K(T(\mathbf{x}, t), W(\mathbf{x}, t)) = K_0[1 + \alpha_T(T(\mathbf{x}, t) - T_0) + \alpha_W(W(\mathbf{x}, t) - W_0)], \tag{64}$$

where K_0 is the compressibility modulus at reference conditions, and α_T and α_W are coefficients of variation of K with respect to T and W. Then, the total pressure, $p(\mathbf{x}, t)$, becomes:

$$\begin{aligned} p(\mathbf{x}, t) = p_0 + K_0[1 + \alpha_T(T(\mathbf{x}, t) - T_0) + \\ = \alpha_W(W(\mathbf{x}, t) - W_0)] \cdot \rho_0[-\beta_T(T(\mathbf{x}, t) - T_0) + \beta_W(W(\mathbf{x}, t) - W_0)]. \end{aligned} \tag{65}$$

Finally, by expanding and simplifying, we obtain:

$$\begin{aligned} p(\mathbf{x}, t) = p_0 + A(T(\mathbf{x}, t) - T_0) + B(W(\mathbf{x}, t) - W_0) + \\ + C(T(\mathbf{x}, t) - T_0)(W(\mathbf{x}, t) - W_0), \end{aligned} \tag{66}$$

where $A = K_0\rho_0\alpha_T - K_0\rho_0\beta_T$, $B = K_0\rho_0\alpha_W + K_0\rho_0\beta_W$, $C = K_0\rho_0(\alpha_T\beta_W + \alpha_W\beta_T)$.
Then, once the distributions of $T(\mathbf{x}, t)$ and $W(\mathbf{x}, t)$ have been obtained, $K(T(\mathbf{x}, t, W(\mathbf{x}, t))$ is computed and then $\rho(\mathbf{x}, t)$ is quantified as specified above.

7.1. Comsol Multiphysics® Implementation

The sonication process, in pretreatment, produced a modest decrease in sludge weight, so a prototype software mixer was designed to reduce the weight of heat-treated sludge more significantly. The numerical model described above was implemented in both steady-state and transient regimes to identify areas within the prototype that were less stressed by the pressure and temperature exerted on the sludge. Results regarding moisture and pressure distribution are obtained over a temperature range of 296.96 K to 377.96 K based on the operating characteristics of the sludge treatment tank.

7.1.1. Some Specifications of the Mixing Tank

Geometrically, it is cylindrical and exhibits rotational symmetry about its longitudinal axis (axial symmetry), implying that every plane section passing through the cylinder's axis is identical, regardless of the rotation angle. Such symmetry reduces the 3D geometric problem to analyzing only a single plane section that includes the cylinder's axis. Since this section faithfully represents the geometry of the entire system, it is not necessary to model the entire 3D domain to study its geometric characteristics. In addition to geometric symmetry, the validity of the reduction is also supported by the fact that the physical conditions are also symmetrical concerning the axis. Reducing the problem from 3D to 2D offers computational advantages by requiring fewer resources than 3D by reducing the number of nodes and elements in the mesh. Figure 4 displays the front and top elevation of the (aluminum) sludge mixing tank in which the conduit required to heat the tank (also aluminum), the 1.4301 stainless steel mixing system, and the high-density (28 kg/m^3) polyethylene outer shell with high thermal insulation properties (λ = 0.04) are evident.

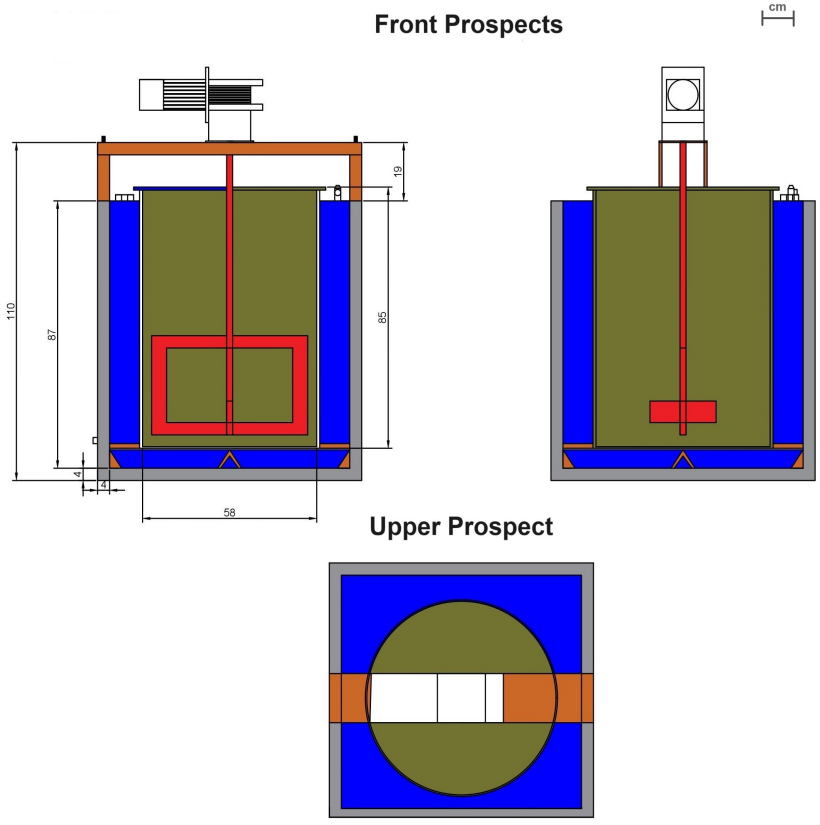

Figure 4. 2D prototype of the sludge treatment tank.

7.1.2. Some Relevant Details About the Designed Mesh

To solve the problem numerically, once the device was implemented geometrically (see Figure 5) under both steady-state and transient conditions, an obtained mesh was constructed using a Delaunay triangulation calibrating it for a fluid dynamics problem whose maximum element size is 0.00335, while their minimum size is around 1.5×10^{-3}. The optimized curvature factor is 0.4, while the maximum element growth ratio is worth 1.2. The obtained mesh has 11,817 degrees of freedom and exhibits high quality since the aspect ratio is $\approx$1, while the skewness is 0. In addition, the smoothness parameter is gradual, and the condition number is minimal, while the Jacobian determinant is positive and stable. The obtained mesh is characterized by 4448 triangular elements and 560 quadrangular

elements. In addition, the number of elements is 588, while those on the vertices are 20. The obtained mesh can be viewed in Figure 6.

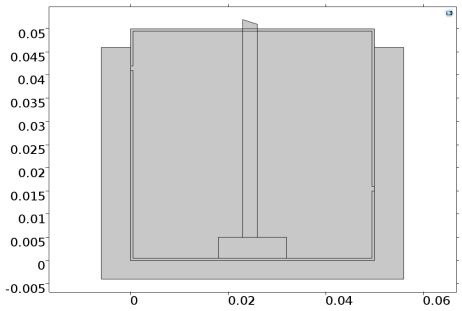

Figure 5. Mixing device designed using FEM for sludge treatment.

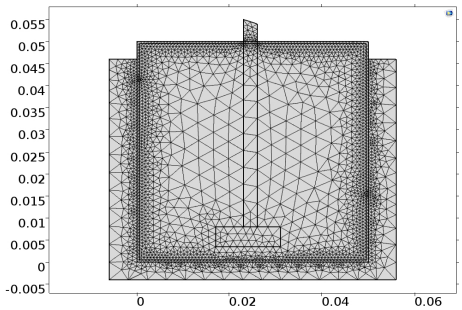

Figure 6. Mesh designed for the analysis of fluid dynamics inside the mixing tank.

Remark 1. *During this study, a preliminary grid independence analysis was performed to ensure that the results obtained using the finite element method were not affected by the density or size of the mesh used. For this purpose, different discretization configurations were considered, varying the maximum size of the grid elements and analyzing the impact on the main parameters of interest, such as temperature, pressure, and humidity distribution within the system. The results showed substantial convergence for an optimized grid, ensuring a balance between accuracy and computational times. Therefore, the chosen mesh configuration was found to be adequate to precisely describe the physical phenomena under consideration without compromising the reliability of the simulations. These checks, although preliminary, confirm the independence of the model with respect to the adopted grid and represent a solid basis for the development of further future studies.*

8. Some Relevant Results

Once the device was implemented, a series of simulations were carried out in both transient and steady state to evaluate the temperature and humidity distribution. However, since the sludge tank is a hermetically sealed aluminum container, to prevent potentially dangerous mechanical instability problems, we equip the pressure control device inside it.

Stationary and Transient Regimes

Simulations in a steady state (temperature and pressure are constant), since the system already reaches the steady state of equilibrium, showed the areas with lower thermal and pressure stresses being less affected by altered environmental conditions, providing valuable indications for the structural stability of the container, eventually.

On the other hand, simulations in the transient regime, during critical phases (startup, heating, and/or cooling of the container as highlighted in Figure 7) showed the evolution of temperature and pressure over time, highlighting how the system responds to rapid or gradual changes in external or internal conditions. In addition, less stressed areas are easily identified as they show fewer thermal and pressure fluctuations, signaling areas of

greater thermal and structural stability. The combined analysis identifies critical stresses; by comparing the results of the two regimes, areas that maintain low stresses in both transient and steady state can be identified, suggesting naturally less stressed regions. Areas that show limited changes in stresses during the transient and stabilize these conditions in the steady-state regime are indicators of structural reliability, with a low probability of deformation or failure.

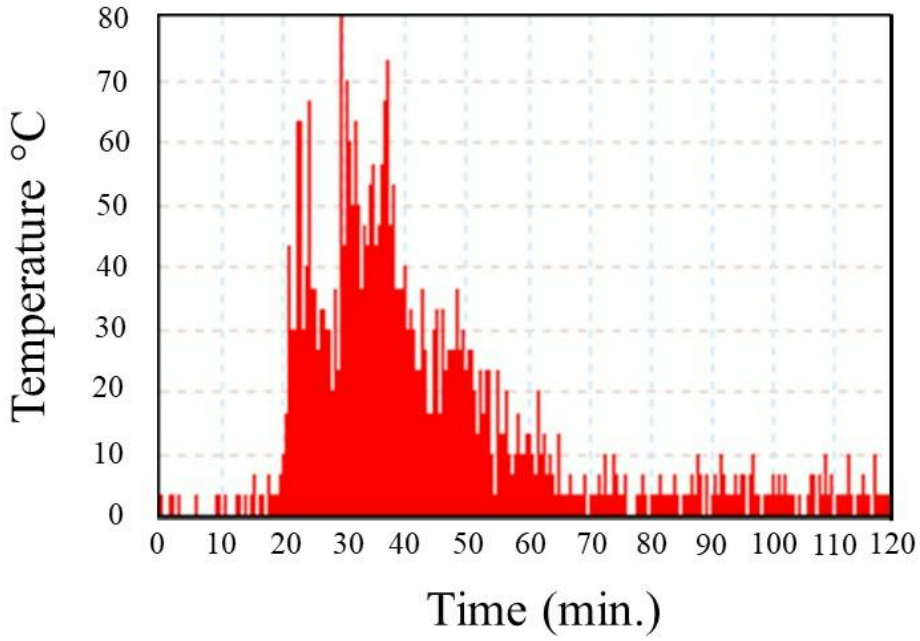

Figure 7. Temperature distribution inside the tank.

Figure 8a displays the areas where the pressure assumes relevant values with apparent overload near the mixer plate (the operating parameters used only listed in Table 4 (please note that the density of the sludge varies with its moisture content during the drying process.). This is in line with expectations since the mixer, being a moving element, undergoes both the action due to the gravity force of the sludge and the effects due to rotation. Obviously, the distribution of the moisture percentage (see Figure 8b) is almost uniform throughout the tank, except in the areas near the mixer plate (tank bottom) where the drying action is more significant.

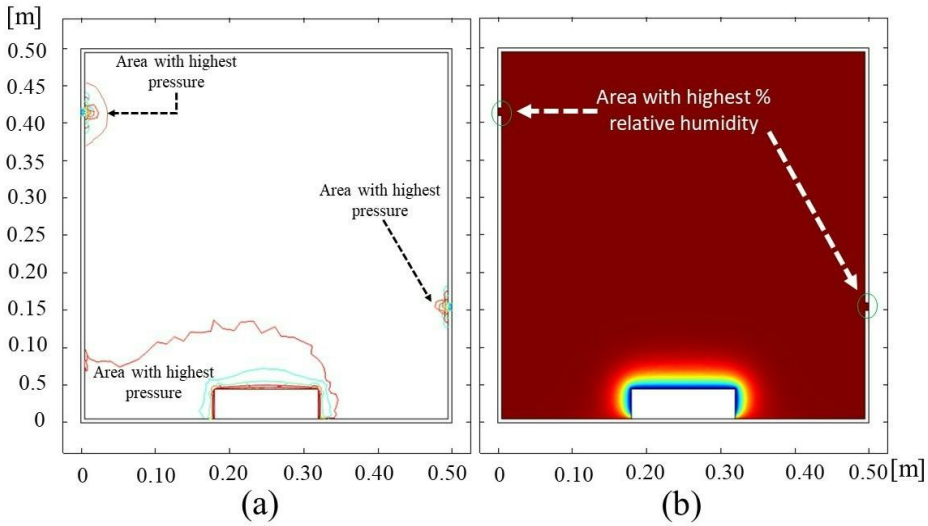

Figure 8. (**a**) Pressure distribution and (**b**) relative humidity inside the sludge-filled tank.

Table 4. Benchmarks for sludge from wastewater.

Parameter	Value	Unit	Note
p_0	101,325	Pa	Standard atmospheric pressure
ρ_0	1050	kg/m^3	Sludge average density
K_0	2.2×10^9	Pa	Water-like compressibility modulus
T_0	293.15	K	Reference temperature (20 °C)
W_0	0.95	kg/kg	Relative humidity (95%)
β_T	2.1×10^{-4}	K^{-1}	Thermal expansion coefficient
β_W	0.05	$(kg/kg)^{-1}$	Variation of density versus humidity
α_T	0.002	K^{-1}	Coefficient of compressibility modulus vs. temperature
α_W	0.01	$(kg/kg)^{-1}$	Variation of compressibility modulus with respect to humidity

9. Prototype for Moisture Detection and Reduction in a Sludge Treatment Tank

Once the system was designed and tested in software mode, we built the prototype for sludge treatment equipped with mechanical and electronic components for proper operation. Specifically, the tank should be connected to a heat source to heat the sludge. The realized prototype, shown in Figure 9 and consisting of the sludge treatment device (a), mixer (b), and sensors placed inside the tank, is insulated by a layer of polystyrene to prevent heat loss. The sludge, coming from the sonication process, is mixed for about 30 min by a mixer operated by a special mechanical component, which is installed above the tank as per the software design. Sensors to measure the mechanical strength of the sludge (to derive the moisture content) were installed inside the treatment tank and placed at the bottom, middle, and top of the tank, as demonstrated by the software analysis. In addition, temperature sensors have been set up so that it is monitored during the heating of the tank to dehydrate the sludge by decreasing its moisture content, allowing a maximum temperature of 110 °C [67]. Finally, for safety benefits, an automatic pressure relief valve is installed that can raise the internal device, allowing excess vapors to escape. The prototype is equipped with a 3PM-0030 impeller agitator (PRO-DO-MIX® Srl Unipersonale), PAdova, Italy) driven by an 18.5 kW three-phase AC motor that provides the necessary power to operate the agitator under any operating condition. Figures 10 and 11 show, respectively, a general and detailed view of the sludge structure before sonification treatment. In Figure 10, a compact and dense structure is clearly observed, with a high viscosity that prevents effective separation of the solid particles from the liquid matrix. This characteristic is typical of raw sludge, in which the presence of particle aggregates and water retention are significant. In Figure 11, a close analysis of the morphology of the sludge highlights a non-uniform grain size distribution, with the presence of agglomerates of variable dimensions and flocculent structures. The non-homogeneous nature of the particles, combined with the presence of lumps and physical-chemical bonds between the components, confirms the difficulty in the dewatering process of untreated sludge. Figure 12 shows the evolution of the sludge structure during ultrasound treatment. The progressive disintegration of the agglomerates is evident, accompanied by a reduction in the viscosity of the material.

Figure 9. Details of the proposed prototype: (**a**) Sludge treatment device; (**b**) Wastewater treatment mixer; (**c**) Mixer and Sensors placed inside the sludge treatment tank

Figure 10. Image of raw sludge before ultrasonic treatment. An aggregated and compact structure is observed, a typical characteristic of untreated sludge, with particles of heterogeneous dimensions and high viscosity.

Figure 11. Close-up view of the sludge morphology before sonification. The non-uniform distribution of the particles and the presence of lumps indicate a slightly disintegrated state with a high tendency to sedimentation.

Figure 12. Distribution of sludge structure during ultrasonic treatment. A gradual disintegration of the agglomerates and a reduction in viscosity are observed, indicative of the cavitational effect induced by sonification, which facilitates the breaking of the particles and the release of intracellular and extracellular materials.

10. Experimental Activity: Some Survey Results

10.1. On the Sonication Process

It is evident, as shown in Figure 13, that high electric currents rapidly stabilize the average particle size, exhibiting a marked decrease of up to 55% in particle size at 1.6 W (corresponding to a 60% amplification of the current), between the 20th and 25th minutes of the sonication treatment. However, the reduction is not pronounced by halving the power (corresponding to an amplification of 40% of the current), standing at 49% in the same time interval. By further reducing the power (0.3 W), the size reduction is around 52% with but between the 30th and 45th minutes (corresponding to current amplification of 20%). As for the ζ potential decreases if the negative surface charge does likewise, providing a clear indication of the stability of the colloids present. As highlighted in Table 5, starting from $\zeta = -11.8$ mV, belonging to the usual range from -10 mV to -30 mV, it showed, after sonication pretreatment, a slight fluctuation with a negative trend as the percentage of applied electric current increased. Since the particles tend to repel each other electrostatically in these cases, it is necessary to add flocculating chemical agents.

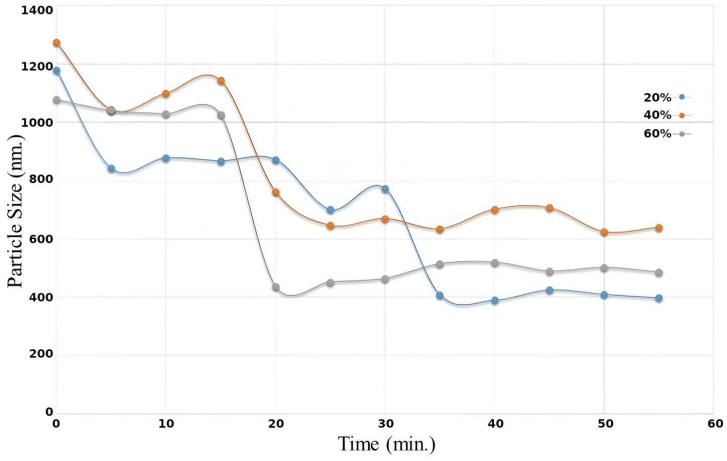

Figure 13. Particle size distribution over time at different amplifications.

Table 5. ζ potential for sludge treated with ultrasound.

Amplification—Treatment Time	Untreated	20% (35 min)	40% (25 min)	60% (25 min)
ζ Potential (mV)	−11.8	−12.2	−11.5	−9.62

Then, as is well known [68], the addition of Ca^{2+} and Mg^{2+} contributes significantly to the flocculation process by neutralizing surface negative charges, as well as by creating ionic bridges between negatively charged particles or between functional groups in the polymer flocculants and the sludge particles by increasing [Ca^{2+}] and [Mg^{2+}] reduces the electric double layer of the particles by decreasing electrostatic repulsion, increasing the attractive van der Waals forces that promote aggregation. However, [Ca^{2+}] and [Mg^{2+}] must be carefully controlled to avoid excess cations that cause very dense or unstable floccules settling rapidly or difficult to separate.

Dispersion agents (non-superactive polymers or highly active substances) added to sludge also prevent sedimentation by deflocculating solids by reducing their viscosity and increasing the amount of dispersible powder material.

To achieve a stable dispersion (ζ potential greater than +30 mV or less than −30 mV), we used the combined effect of Silcosperse HLD5 at 3% v/v, silicon-free high-performance for water-based pigmented systems (total solids: 49.0–51.0%; active agent: 39.0–41.0%; pH: 7.0–9.0, with the ultrasound treatment (Table 6).

Table 6. ζ potential and conductivity for sludges containing a dispersing agent and treated with US.

Current Percentage Treatment Time	20% (35 min)	40% (25 min)	60% (25 min)	Silcosperse (%w/v)	Conductivity (mS/cm)
ζ potential (mV)					
−12.3	−11.8	−11.5	−14.8	1.0	1.28
−11.1	−12.2	−12.1	−15.2	1.5	1.19
−12.5	−11.6	−12.3	−14.9	3.0	1.20

The results confirmed that the above combination of treatments produces stable dispersion by improving the interaction between US and sludge. The additive allows the sludge to become conductive. Since the additive allows the sludge to become conductive, as its concentration increases, conductivity increases.

The effectiveness of sludge disintegration and solubilization was monitored by observing COD trends in the sludge supernatant.

10.2. On COD Values and Specific Gravity Reduction

Treatment of samples with US increases COD value, indicating a high content of oxidizable organic material in the sample due to disintegration. COD is around 2012 mg/L for untreated sludge, while 35 min of sonication increases to 2200 mg/L with ζ of 20%. If we then perform a 25-minute sonication, COD is around 3534 mg/L with ζ of 40% and 3429 mg/L with ζ of 60%. As previously observed in batch experiments, treatment by ultrasound increases COD value, indicating a high content of oxidizable organic material in the sample due to the disintegration process. In the case of the pre-industrial prototype test, a better efficiency of the disintegration process is noted in Table 7.

In the same frequency range, sonication tests were performed to evaluate the impact of the treatment in the sludge drying phase. The disintegration process, induced by sonication, fragments the sludge particles into smaller units, promoting steam migration to the surface and reducing particle aggregation during the drying process. The results, shown in Table 8,

show a slight reduction in specific gravity of between 1 and 2% compared to the untreated and dried samples under identical experimental conditions (from 34.02 g to 34.01 g) due to the reduced moisture content of the sonicated sample.

Table 7. COD absolute and percentage change obtained during the pretreatment phase carried out in the laboratory with a sludge volume (sewage sludge) of 125 mL and during the use of the pretreatment prototype industrial installed in the sewage treatment plant for the treatment of a sludge volume equal to 8 L.

	Test in Batch (V = 125 mL)	**Testing with Pre-Industrial Prototype (V = 8 L)**
COD—Initial (mg/L)	2000	66
COD—Final (mg/L)	3500	552
Variation (%)	+75	+736

Table 8. Sludge drying test comparing untreated sludge and ultrasonically treated sludge (60% amplification).

Sample Type	**Initial Weight (g)**	**Weight Reduction (%)**
Untreated sludge	37.52	9.32
Sludge treated with US (60% A)	38.04	10.61

10.3. On the Reduction of Sludge Weight

The results obtained during the measurement campaign showed a further percentage reduction in sludge weight. Specifically, the sludge treated in the tank had an initial weight of 38.05 g and a final weight of 33.52 g, resulting in a percentage reduction in weight of 11.91%. The samples were treated at about 105°C in the sludge treatment tank for 2 h (see Figure 14). Comparing the initial and final weight data of the pretreated, US, and tank-treated sludge, the trend shown in Figure 15 emerges.

Figure 14. Prototype of a sludge mixing tank. Sludge, once sonicated, is deposited in a conveyor belt and fed into the prototype. Equipped with a temperature sensor and a humidity sensor, the prototype mixing tank heats the already ultrasonically treated sludge, further reducing the amount of water and consequently making it lighter.

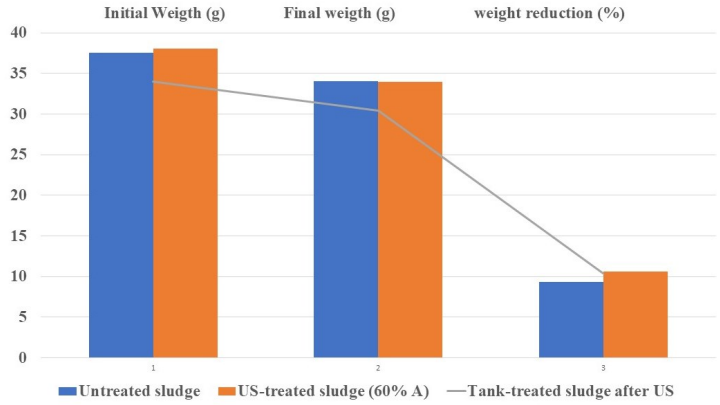

Figure 15. Untreated Sludge (Blue)—US (Orange)—Prototype Heat Source (Grey).

The trend shown indicates a slight decrease in the percentage of sludge weight reduction when using the prototype whose exclusive use results in higher energy consumption than the joint use with US pretreatment. As shown in Figure 15, the combination of sonication with heat treatment leads to a significant reduction in the heating rate of the pretreated sludge material.

10.4. On the Reduction of Water Content

Finally, the final water content of dry sludge was studied and analyzed, revealing that sonication alone is inadequate for effective sludge conditioning, making it necessary to combine with heat treatment by reducing the water content by 9%.

Remark 2. *It is important to note that, in addition to evaluating the ζ potential and conductivity, further sludge characteristics were analyzed to assess the treatment effects. Before sonification, the sludge exhibited a compact morphology with a non-uniform particle distribution and cohesive agglomerates, as shown in Figures 10 and 11. During ultrasound treatment, the cavitational effect progressively disintegrated these structures, facilitating the release of intracellular and extracellular materials (Figure 12). The increase in chemical oxygen demand (COD) observed during sonification indicates enhanced bioavailability of organic components and improved biodegradability, beneficial for subsequent biological processes. Additionally, the combination of sonification and thermal treatment led to a moisture content reduction, resulting in an 11–12% decrease in sludge weight, as highlighted in Figure 12. These findings confirm the process's effectiveness in improving sludge manageability and its suitability for agricultural applications.*

11. Comparison with Some Known Scenarios in Literature

The following simplifications have been considered in our numerical implementation. First, we have not considered some microflows (polymer thickening and dehydration). On the contrary, we considered it appropriate to include both nitrogen dioxide and sulfur dioxide emissions in the combined heat and power production.

Analysis and Optimization of Nutrient and Energy Recovery from Sludge: Comparison of Composting and Anaerobic Digestion

The scenarios studied in [69,70] assumed that all digested compounds and products would be used as fertilizers or soil conditioners for agricultural purposes to calculate the maximum nutrient recovery and energy recovery efficiency. Four processes were selected in combination for composting and soil application: thickening, dewatering, composting, and soil application. After pretreatment, the dewatered sludge is started for composting,

requiring a 50% reduction in sludge weight, about 645 kg of reaction oxygen, and a total of 1975 kg of wood chips as filling agent, including 395 kg of raw chips and 1580 recycled chips. In combination with anaerobic digestion, land application, and cogeneration, there are five processes: dewatering, anaerobic digestion, digestion, land application, and cogeneration. According to the first method, raw sludge undergoes pretreatment, reducing the weight of expanded sludge by 1/3 with considerable water expenditure. Next, the sludge is subjected to anaerobic digestion, yielding two main products: 98.6% raw digestate and 1.4% biogas. The sludge output possesses the characteristics shown in Table 9.

Table 9. Characterization of the sludge processed and leaving the plant.

Heavy Metals [mg/Kg]	Sludge Analysis	Heavy Metals [mg/Kg]	Sludge Analysis
Copper	217–247	Zinc	203–357
Cadmium	<1	Mercury	<1
Lead	24–43	Nickel	17–30

Classifying the treated sludge, as opposed to the incoming sludge, allows it to be used in the agricultural sector because it meets the parameters required by current regulations. The raw digestate undergoes further dewatering, and the resulting by-products are transported and spread on agricultural land. At the same time, the generated biogas is directed to a cogeneration plant for energy recovery [71]. The fusion of anaerobic digestion, land application, and biogas involves six processes, of which the first four mirror those of the second method presented. The unique feature lies in the treatment of biogas carried out by this method through the purification of biogas and the subsequent utilization of energy. About 41.3% of the biogas is transformed into biomethane, while 48.7% of the CO_2 is removed. The theoretically required amount of oxygen for the combustion of 41.3% biomethane is four times higher [72]. The disintegration process can be achieved thermally (at 170–190 °C for 30–60 min), resulting in substantial solubilization along with a transformation of the sludge characteristics. This leads to a significant improvement in filterability and a reduction in pathogens [73]. Literature methods indicate that the product of the former method boasts the highest relative nutrient recovery efficiency due to its small volume and low water content compared to digestate. However, composting is constrained by its inherent limitations in that it cannot harness the energy content of sludge, making its energy contribution negligible. This represents a significant disadvantage of composting. The performance of anaerobic digestion is more complete, although its relative nutrient recovery efficiency is lower than that of composting. Compared with composting technology, anaerobic digestion is more energy efficient and has less environmental impact. The latter methodology shares a similar energy recovery efficiency as the former but exceeds it in environmental impact. Therefore, from an overall perspective, the combination of anaerobic digestion, agricultural application, and cogeneration should be considered the most optimal. However, all methods presented require intensive electricity consumption. Contrary to the literature's findings, the research demonstrates both effective sludge weight reduction and reasonable energy consumption. Conventional systems suffer energy losses due to frictional heat, especially with high-pressure pumps and blade mixers that create turbulence during processing. These turbulences lead to friction between the liquid particles and the vibrating parts of the equipment, converting the input energy into frictional heating, which is lost and does not contribute to the dispersion effects. The stronger the cavitation forces that exert stress on the particles, the less energy is required for effective dispersion [74]. Finally, the sludge mixer, designed to reduce the water content in the sludge further, operates based on energy-harvesting techniques [75,76]. It is worth noting

that the results obtained meet all normative requirements (UNI EN 13657:2004+ UNI EN ISO 11885:2009 method; UNI 10802-04, UNI 12457-2:04, and UNI EN ISO 11885:09 methods; UNI EN 13657:2004 and UNI EN ISO 11885:2009 methods). Scrupulous adherence to the mentioned standards ensures that the procedures adopted are reliable and consistent with the reference standards, confirming the quality and reliability of the analyses performed.

12. Conclusions

This study introduced an innovative approach for sewage sludge treatment, combining ultrasonic and thermal treatments to optimize sludge management for agricultural purposes. The results demonstrated significant improvements in treatment efficiency, with several key advantages summarized below:

- **Reduction of moisture content and improved stability**: The ultrasonic treatment, combined with thermal techniques, achieved a moisture content reduction of up to 20%. This improvement enhanced material stability, making it more suitable for agricultural use or further processing.
- **Increased energy efficiency**: Compared to traditional methods, the proposed protocol reduced energy consumption by up to 60%, demonstrating that ultrasonic techniques can offer a cost-effective and environmentally sustainable solution for sludge treatment.
- **Environmental benefits**: The method significantly reduced greenhouse gas emissions, human toxicity, and fossil fuel consumption, aligning the process with principles of circular economy and environmental sustainability.
- **Validation at scale and practical applicability**: The protocol was validated both in laboratory and real-plant settings, confirming its feasibility for large-scale implementation in wastewater treatment systems. The proposed methodology adapts to industrial contexts without requiring costly structural interventions.

In addition to these direct benefits, the study highlighted the effectiveness of the developed mathematical model, which integrates information on temperature, humidity, and pressure to optimize operational parameters. This approach enables scientifically supported treatment management, reducing operational costs and improving the quality of the final product. Despite the promising results, the study identified some limitations, including the need to improve the prototype's reliability during operation and address some energy efficiency issues. Future developments will focus on refining the prototype, testing processes on different types of sludge, and implementing advanced monitoring systems based on soft computing technologies to ensure continuous control of the treated material composition. In summary, the presented work addresses existing gaps in the literature, providing an innovative and sustainable solution for sewage sludge treatment. This study offers a solid foundation for further developments and applications in the wastewater treatment sector.

Author Contributions: Conceptualization, F.L., S.A.P., G.A. and M.V.; methodology, F.L., S.A.P., G.A. and M.V.; software, F.L., S.A.P., G.A. and M.V.; validation, F.L., S.A.P., G.A. and M.V.; formal analysis, F.L., S.A.P., G.A. and M.V.; investigation, F.L., S.A.P., G.A. and M.V.; resources, F.L., S.A.P., G.A. and M.V.; data curation, F.L., S.A.P., G.A. and M.V.; writing—original draft preparation, F.L., S.A.P., G.A. and M.V.; writing—review and editing, F.L., S.A.P., G.A. and M.V.; visualization, F.L., S.A.P., G.A. and M.V.; supervision, F.L., S.A.P., G.A. and M.V.; project administration, F.L., S.A.P., G.A. and M.V.; funding acquisition, F.L., S.A.P., G.A. and M.V. All authors have read and agreed to the published version of the manuscript.

Funding: This research has been supported by the Italian Ministry of University and Research under the Program PRIN 2022: "Integration of Artificial Intelligence and Ultrasonic Techniques for Monitoring Control and Self-Repair of Civil Concrete Structures (CAIUS)"—Code 2022AZPLL8.

Institutional Review Board Statement: Not applicable.

Informed Consent Statement: Not applicable.

Data Availability Statement: Data are contained within the article.

Conflicts of Interest: The authors declare no conflicts of interest.

Abbreviations

The following abbreviations are used in this manuscript:

US	Ultrasonic
FEM	Finite Element Method
COD	Chemical Oxygen Demand

References

1. Rajendran, S.; Priya, T.A.K.; Khoo, K.S.; Hoang, K.T.; Ng, H.S.; Munawaroh, H.S.H.; Show, P.L. A Critical Review on Various Remediation Approaches for Heavy Metal Contaminants Removal from Contaminated Soils. *Chemosphere* **2022**, *287*, 132369. https://doi.org/10.1016/j.chemosphere.2021.132369.
2. Rabie, G.M.; Abd El-Halim, H.; Rozaik, E.H. Influence of Using Dry and Wet Wastewater Sludge in Concrete Mix on Its Physical and Mechanical Properties. *Ain Shams Eng. J.* **2019**, *10*, 705–712. https://doi.org/10.1016/j.asej.2018.10.009.
3. Sharma, B.; Sarkar, A.; Singh, P.; Singh, R.P. Agricultural Utilization of Biosolids: A Review on Potential Effects on Soil and Plant Growth. *Waste Manag.* **2017**, *64*, 117–132. https://doi.org/10.1016/j.wasman.2017.03.002.
4. Liu, Y.; Joo-Hwa, T. Strategy for Minimization of Excess Sludge Production from the Activated Sludge Process. *Biotechnol. Adv.* **2001**, *19*, 97–107. https://doi.org/10.1016/S0734-9750(00)00066-5.
5. Sodhi, V.; Bansal, A.; Jha, M.K. Minimization of Excess Bio-Sludge and Pollution Load in Oxic-Settling-Anaerobic Modified Activated Sludge Treatment for Tannery Wastewater. *J. Clean. Prod.* **2020**, *243*, 118492. https://doi.org/10.1016/j.jclepro.2019.118492.
6. Corsino, S.F.; de Oliveira, T.S.; Di Trapani, D.; Torregrossa, M.; Viviani, G. Simultaneous Sludge Minimization, Biological Phosphorous Removal, and Membrane Fouling Mitigation in a Novel Plant Layout for MBR. *J. Environ. Manag.* **2020**, *259*, 109826. https://doi.org/10.1016/j.jenvman.2019.109826.
7. Massé, D.I.; Croteau, F.; Massé, L. The Fate of Crop Nutrients during Digestion of Swine Manure in Psychrophilic Anaerobic Sequencing Batch Reactors. *Bioresour. Technol.* **2007**, *98*, 2819–2823. https://doi.org/10.1016/j.biortech.2006.07.040.
8. Wu, B.; Xiaohu, D.; Xiaoli, C. Critical Review on Dewatering of Sewage Sludge: Influential Mechanism, Conditioning Technologies, and Implications to Sludge Re-Utilizations. *Water Res.* **2020**, *180*, 115912. https://doi.org/10.1016/j.watres.2020.115912.
9. Collivignarelli, M.C.; Miino, M.C.; Cillari, G.; Bellazzi, S.; Caccamo, F.M.; Abbà, A.; Bertanza, G. Estimation of Thermal Energy Released by Thermophilic Biota during Sludge Minimization in a Fluidized Bed Reactor: Influence of Anoxic Conditions. *Process Saf. Environ. Prot.* **2022**, *166*, 249–256. https://doi.org/10.1016/j.psep.2022.08.022.
10. Mrozik, W.; Rajaeifar, M.A.; Heidrich, O.; Christensen, P. Environmental Impacts, Pollution Sources, and Pathways of Spent Lithium-Ion Batteries. *Energy Environ. Sci.* **2021**, *14*, 6099–6121. https://doi.org/10.1039/D1EE00691F.
11. Øegaard, H. Sludge Minimization Technologies—An Overview. *Water Sci. Technol.* **2004**, *49*, 31–40. https://doi.org/10.2166/wst.2004.0604.
12. Bagheri, M.; Bauer, T.; Burgman, L.E.; Wetterlund, E. Fifty Years of Sewage Sludge Management Research: Mapping Researchers' Motivations and Concerns. *J. Environ. Manag.* **2023**, *325*, 116412. https://doi.org/10.1016/j.jenvman.2022.116412.
13. Fiorillo, A.S.; Grimaldi, D.; Paolino, D.; Pullano, S.A. Low-Frequency Ultrasound in Medicine: An In Vivo Evaluation. *IEEE Trans. Instrum. Meas.* **2012**, *61*, 1658–1663. https://doi.org/10.1109/TIM.2012.2188350.
14. Liu, Z.; Luo, F.; He, L.; Wang, S.; Wu, Y.; Chen, Z. Physical Conditioning Methods for Sludge Deep Dewatering: A Critical Review. *J. Environ. Manag.* **2024**, *360*, 121207. https://doi.org/10.1016/j.jenvman.2024.121207.
15. Yuan, H.; Zhu, N. Progress of Improving Waste Activated Sludge Dewaterability: Influence Factors, Conditioning Technologies and Implications and Perspectives. *Sci. Total Environ.* **2023**, 168605. https://doi.org/10.1016/j.scitotenv.2023.168605.
16. Ma, H.P.; Li, J.P.; Hu, X.P.; Xie, L.; An, G.; Chen, J.Q.; Lv, W.J. On-Site Source-Separation of Microparticles and Reuse of Coal Gasification Wastewater via a Micro-Channel Separator: Performance and Separation Mechanism. *Sep. Purif. Technol.* **2024**, *341*, 126565. https://doi.org/10.1016/j.seppur.2024.126565.
17. Zhang, X.; Ye, P.; Wu, Y. Enhanced Technology for Sewage Sludge Advanced Dewatering from an Engineering Practice Perspective: A Review. *J. Environ. Manag.* **2022**, *321*, 115938. https://doi.org/10.1016/j.jenvman.2022.115938.
18. Hou, J.; Hong, C.; Ling, W.; Hu, J.; Feng, W.; Xing, Y.; Feng, L. Research Progress in Improving Sludge Dewaterability: Sludge Characteristics, Chemical Conditioning and Influencing Factors. *J. Environ. Manag.* **2024**, *351*, 119863. https://doi.org/10.1016/j.jenvman.2023.119863

19. Laganà, F.; De Carlo, D.; Calcagno, S.; Pullano, S. A.; Critello, D.; Falcone, F.; Fiorillo, A. S. Computational model of cell deformation under fluid flow based rolling. In Proceedings of the 2019 E-Health and Bioengineering Conference (EHB), Iasi, Romania, 21–23 November 2019; pp. 1–4. https://doi.org/10.1109/EHB47216.2019.8970065.
20. Hao, X.; Chen, Q.; van Loosdrecht, M.C.; Li, J.; Jiang, H. Sustainable Disposal of Excess Sludge: Incineration Without Anaerobic Digestion. *Water Res.* **2020**, *170*, 115298. https://doi.org/10.1016/j.watres.2019.115298.
21. Muhlack, R.A.; Potumarthi, R.; Jeffery, D.W. Sustainable Wineries Through Waste Valorisation: A Review of Grape Marc Utilisation for Value-Added Products. *Waste Manag.* **2018**, *72*, 99–118. https://doi.org/10.1016/j.wasman.2017.11.011.
22. Wang, J.; Lai, Y.; Wang, X.; Ji, H. Advances in Ultrasonic Treatment of Oily Sludge: Mechanisms, Industrial Applications, and Integration with Combined Treatment Technologies. *Environ. Sci. Pollut. Res.* **2024**, *31*, 14466–14483. https://doi.org/10.1007/s11356-024-32089-4.
23. Askarniya, Z.; Sun, X.; Wang, Z.; Boczkaj, G. Cavitation-Based Technologies for Pretreatment and Processing of Food Wastes: Major Applications and Mechanisms–A Review. *Chem. Eng. J.* **2023**, *454*, 140388. https://doi.org/10.1016/j.cej.2022.140388.
24. Hou, T.; Song, H.; Cui, Z.; He, C.; Liu, L.; Li, P.; Jiao, Y. Nanobubble Technology to Enhance Energy Recovery from Anaerobic Digestion of Organic Solid Wastes: Potential Mechanisms and Recent Advancements. *Sci. Total Environ.* **2024**, *931*, 172885. https://doi.org/10.1016/j.scitotenv.2024.172885.
25. Wang, T.; Yang, C.; Sun, P.; Wang, M.; Lin, F.; Fiallos, M.; Khu, S.T. Generation Mechanism of Hydroxyl Free Radicals in Micro–Nanobubbles Water and Its Prospect in Drinking Water. *Processes* **2024**, *12*, 683. https://doi.org/10.3390/pr12040683.
26. Wang, H.; Liu, X.; Zhang, Z. Approaches for Electroplating Sludge Treatment and Disposal Technology: Reduction, Pretreatment and Reuse. *J. Environ. Manag.* **2024**, *349*, 119535. https://doi.org/10.1016/j.jenvman.2023.119535.
27. Zeng, H.; Liu, C.; Wang, F.; Zhang, J.; Li, D. Disposal of Iron-Manganese Sludge from Waterworks and Its Potential for Arsenic Removal. *J. Environ. Chem. Eng.* **2022**, *10*, 108480. https://doi.org/10.1016/j.jece.2022.108480.
28. Zeng, S.; Li, M.; Li, G.; Lv, W.; Liao, X.; Wang, L. Innovative Applications, Limitations and Prospects of Energy-Carrying Infrared Radiation, Microwave and Radio Frequency in Agricultural Products Processing. *Trends Food Sci. Technol.* **2022**, *121*, 76–92. https://doi.org/10.1016/j.tifs.2022.01.011.
29. Feng, Y.; Tao, Y.; Meng, Q.; Qu, J.; Ma, S.; Han, S.; Zhang, Y. Microwave-Combined Advanced Oxidation for Organic Pollutants in the Environmental Remediation: An Overview of Influence, Mechanism, and Prospective. *Chem. Eng. J.* **2022**, *441*, 135924. https://doi.org/10.1016/j.cej.2022.135924.
30. Yakamercan, E.; Bhatt, P.; Aygun, A.; Adesope, A.W.; Simsek, H. Comprehensive Understanding of Electrochemical Treatment Systems Combined with Biological Processes for Wastewater Remediation. *Environ. Pollut.* **2023**, *330*, 121680. https://doi.org/10.1016/j.envpol.2023.121680.
31. Ahmed, M.; Mavukkandy, M.O.; Giwa, A.; Elektorowicz, M.; Katsou, E.; Khelifi, O.; Hasan, S.W. Recent Developments in Hazardous Pollutants Removal from Wastewater and Water Reuse Within a Circular Economy. *NPJ Clean Water* **2022**, *5*, 12. https://doi.org/10.1038/s41545-022-00154-5.
32. Pavel, M.; Anastasescu, C.; State, R.N.; Vasile, A.; Papa, F.; Balint, I. Photocatalytic Degradation of Organic and Inorganic Pollutants to Harmless End Products: Assessment of Practical Application Potential for Water and Air Cleaning. *Catalysts* **2023**, *13*, 380. https://doi.org/10.3390/catal13020380.
33. Ahmadi, Y.; Kim, K.H. Modification Strategies for Visible-Light Photocatalysts and Their Performance-Enhancing Effects on Photocatalytic Degradation of Volatile Organic Compounds. *Renew. Sustain. Energy Rev.* **2024**, *189*, 113948. https://doi.org/10.1016/j.rser.2023.113948.
34. Tunçal, T.; Mujumdar, A.S. Modern Techniques for Sludge Dewaterability Improvement. *Dry. Technol.* **2022**, *41*, 339–351. https://doi.org/10.1080/07373937.2022.2092127.
35. Kolya, H.; Kang, C.W. Bio-Based Polymeric Flocculants and Adsorbents for Wastewater Treatment. *Sustainability* **2023**, *15*, 9844. https://doi.org/10.3390/su15129844.
36. Lin, W.; Liu, X.; Ding, A.; Ngo, H.H.; Zhang, R.; Nan, J.; Li, G. Advanced Oxidation Processes (AOPs)-Based Sludge Conditioning for Enhanced Sludge Dewatering and Micropollutants Removal: A Critical Review. *J. Water Process Eng.* **2022**, *45*, 102468. https://doi.org/10.1016/j.jwpe.2021.102468.
37. Myszograj, S.; Płuciennik-Koropczuk, E. Thermal Disintegration of Sewage Sludge as a Method of Improving the Biogas Potential. *Energies* **2023**, *16*, 559. https://doi.org/10.3390/en16010559.
38. Pilli, S.; Bhunia, P.; Yan, S.; LeBlanc, R.J.; Tyagi, R.D.; Surampalli, R.Y. Ultrasonic Pretreatment of Sludge: A Review. *Ultrason. Sonochem.* **2011**, *18*, 1–18. https://doi.org/10.1016/j.ultsonch.2010.02.014.
39. Djellabi, R.; Su, P.; Ambaye, T.G.; Cerrato, G.; Bianchi, C.L. Ultrasonic Disintegration of Municipal Sludge: Fundamental Mechanisms, Process Intensification and Industrial Sono-Reactors. *ChemPlusChem* **2024**, *89*, e202400016. https://doi.org/10.1002/cplu.202400016.

40. Shah, A.A.; Walia, S.; Kazemian, H. Advancements in Combined Electrocoagulation Processes for Sustainable Wastewater Treatment: A Comprehensive Review of Mechanisms, Performance, and Emerging Applications. *Water Res.* **2024**, *252*, 121248. https://doi.org/10.1016/j.watres.2024.121248.
41. Angiulli, G.; Calcagno, S.; De Carlo, D.; Laganà, F.; Versaci, M. Second-Order Parabolic Equation to Model, Analyze, and Forecast Thermal-Stress Distribution in Aircraft Plate Attack Wing–Fuselage. *Mathematics* **2019**, *8*, 6. https://doi.org/10.3390/math8010006.
42. Gherghel, A.; Teodosiu, C.; De Gisi, S. A Review on Wastewater Sludge Valorisation and Its Challenges in the Context of Circular Economy. *J. Clean. Prod.* **2019**, *228*, 244–263. https://doi.org/10.1016/j.jclepro.2019.04.240.
43. Zheng, M.; Hu, Z.; Liu, T.; Sperandio, M.; Volcke, E.I.; Wang, Z.; Yuan, Z. Pathways to Advanced Resource Recovery from Sewage. *Nat. Sustain.* **2024**, *7*, 1395–1404. https://doi.org/10.1038/s41893-024-01423-6.
44. Witek-Krowiak, A.; Gorazda, K.; Szopa, D.; Trzaska, K.; Moustakas, K.; Chojnacka, K. Phosphorus Recovery from Wastewater and Bio-Based Waste: An Overview. *Bioengineered* **2022**, *13*, 13474–13506. https://doi.org/10.1080/21655979.2022.2077894.
45. Shaddel, S.; Bakhtiary-Davijany, H.; Kabbe, C.; Dadgar, F.; Østerhus, S.W. Sustainable Sewage Sludge Management: From Current Practices to Emerging Nutrient Recovery Technologies. *Sustainability* **2019**, *11*, 3435. https://doi.org/10.3390/su11123435.
46. Zeng, Q.; Huang, H.; Tan, Y.; Chen, G.; Hao, T. Emerging Electrochemistry-Based Process for Sludge Treatment and Resources Recovery: A Review. *Water Res.* **2022**, *209*, 117939. https://doi.org/10.1016/j.watres.2021.117939.
47. Espinoza, J.R.; Lizama, A.C.; Palma, R.Y.; Hernández-Martínez, G.; Youssef, C.B.; Pedreguera, A.Z. Ultrasonic Pretreatment of Sewage Sludge, an Effective Tool to Improve the Anaerobic Digestion: Current Challenges, Recent Developments, and Perspectives. In *Development in Waste Water Treatment Research and Processes*; Elsevier: Amsterdam, The Netherlands, 2022; pp. 119–138. https://doi.org/10.1016/B978-0-323-85584-6.00009-1.
48. Goldan, E.; Nedeff, V.; Barsan, N.; Culea, M.; Tomozei, C.; Panainte-Lehadus, M.; Mosnegutu, E. Evaluation of the Use of Sewage Sludge Biochar as a Soil Amendment—A Review. *Sustainability* **2022**, *14*, 5309. https://doi.org/10.3390/su14095309.
49. Zhang, Y.; Ling, Z.; Zhao, M.; Sha, L.; Li, C.; Lu, X. Investigation of the Properties and Mechanism of Activated Sludge in Acid-Magnetic Powder Conditioning and Vertical Pressurized Electro-Dewatering (AMPED) Process. *Sep. Purif. Technol.* **2024**, *328*, 124973. https://doi.org/10.1016/j.seppur.2023.124973.
50. Mehrez, K.; Fryda, L.; Visser, R.; Kane, A.; Leblanc, N.; Djelal, H. Hydrothermal Processes of Contaminated Biomass: Fate of Heavy Metals and Liquid Effluent Valorization. *Biomass Convers. Biorefin.* **2024**, *8*, 1–16. https://doi.org/10.1007/s13399-024-06023-0.
51. Pasalari, H.; Farzadkia, M.; Khosravani, F.; Ganachari, S.; Aminabhavi, T.M. Phosphorus Recovery from Sewage Sludge via Chemical and Thermal Technologies. *Chem. Eng. J.* **2024**, *496*, 153869. https://doi.org/10.1016/j.cej.2024.153869.
52. Ambaye, T.G.; Djellabi, R.; Vaccari, M.; Prasad, S.; Aminabhavi, T.M.; Rtimi, S. Emerging Technologies and Sustainable Strategies for Municipal Solid Waste Valorization: Challenges of Circular Economy Implementation. *J. Clean. Prod.* **2023**, *423*, 138708. https://doi.org/10.1016/j.jclepro.2023.138708.
53. Nguyen, T.A.H.; Bui, T.H.; Guo, W.S.; Ngo, H.H. Valorization of the Aqueous Phase from Hydrothermal Carbonization of Different Feedstocks: Challenges and Perspectives. *Chem. Eng. J.* **2023**, *472*, 144802. https://doi.org/10.1016/j.cej.2023.144802.
54. Leal, C.; del Río, A.V.; Mesquita, D.P.; Amaral, A.L.; Castro, P.M.; Ferreira, E.C. Sludge Volume Index and Suspended Solids Estimation of Mature Aerobic Granular Sludge by Quantitative Image Analysis and Chemometric Tools. *Sep. Purif. Technol.* **2020**, *234*, 116049. https://doi.org/10.1016/j.seppur.2019.116049.
55. Martínez, E.J.; Rosas, J.G.; Morán, A.; Gómez, X. Effect of Ultrasound Pretreatment on Sludge Digestion and Dewatering Characteristics: Application of Particle Size Analysis. *Water* **2015**, *7*, 6483–6495. https://doi.org/10.3390/w7116483.
56. Morabito, F.C. Independent Component Analysis and Feature Extraction Techniques for NdT Data. Mater. Eval. **2000**, *58*, 85–92.
57. Liu, F.; Chen, C.; Qian, J. Film-Like Bacterial Cellulose/Cyclodextrin Oligomer Composites with Controllable Structure for the Removal of Various Persistent Organic Pollutants from Water. *J. Hazard. Mater.* **2021**, *405*, 124122.
58. Zaki, N.; Hadoudi, N.; Charki, A.; Bensitel, N.; Ouarghi, H.E.; Amhamdi, H.; Ahari, M. H. Advancements in the Chemical Treatment of Potable Water and Industrial Wastewater Using the Coagulation–Flocculation Process. *Sep. Sci. Technol.* **2023**, *58*, 2619–2630.
59. Rovira, J.; Mari, M.; Nadal, M.; Schuhmacher, M.; Domingo, J.L. Use of Sewage Sludge as Secondary Fuel in a Cement Plant: Human Health Risks. *Environ. Int.* **2011**, *37*, 105–111. https://doi.org/10.1016/j.envint.2010.08.001.
60. Kebe, X.; Abbt-Braun, G.; Horn, H. Changes in the Characteristics of Dissolved Organic Matter During Sludge Treatment: A Critical Review. *Water Res.* **2000**, *187*, 116441. https://doi.org/10.1016/j.watres.2020.116441.
61. Munafò, C.F.; Palumbo, A.; Versaci, M. An Inhomogeneous Model for Laser Welding of Industrial Interest. *Mathematics* **2023**, *11*, 3357. https://doi.org/10.3390/math11153357
62. Versaci, M.; Laganà, F.; Morabito, F.C.; Palumbo, A.; Angiulli, G. Adaptation of an Eddy Current Model for Characterizing Subsurface Defects in CFRP Plates Using FEM Analysis Based on Energy Functional. *Mathematics* **2024**, *12*, 2854. https://doi.org/10.3390/math12182854

63. Versaci, M.; Angiulli, G.; Fattorusso, L.A.; Di Barba, P.; Jannelli, A. Galerkin-FEM Approach for Dyynamic Recovering of the Plate Profile in Electrostatic MEMS with Fringing Field. *COMPEL-Int. J. Comput. Math. Electr. Electron. Eng.* **2024**, *43*, 744–770. https://doi.org/10.1108/COMPEL-11-2023-0556
64. Burrascano, P.; Di Schino, A.; Versaci, M. Efficient Estimation of Synthetic Indicators for the Assessment of Nonlinear Systems Quality. *Appl. Sci.* **2024**, *14*, 9259. https://doi.org/10.3390/app14209259
65. Versaci, M.; Angiulli, G.; La Foresta, F.; Laganà, F.; Palumbo, A. Intuitionistic Fuzzy Divergence for Evaluating the Mechanical Stress State of Steel Plates Subject to Bi-Axial Loads. *Integr. Comput.-Aided Eng. Link Disabl.* **2024**, *31*, 363–379.
66. Angiulli, G.; Calcagno, S.; La Foresta, F.; Versaci, M. Concrete Compressive Strength Prediction Using Combined Non-Destructive Methods: A Calibration Procedure Using Preexisting Conversion Models Based on Gaussian Process Regression. *J. Compos. Sci.* **2024**, *8*, 300. https://doi.org/10.3390/jcs8080300
67. Pellicanò, D.; Calcagno, S.; De Carlo, D.; Laganà, F. Analysis and Study of an Integrated System Based on Eddy Current for the Osteogenesis Process. In Proceedings of the 2023 International Workshop on Biomedical Applications, Technologies and Sensors (BATS), Catanzaro, Italy, 28–29 September 2023; pp. 89–94. https://doi.org/10.1109/BATS59463.2023.10303224.
68. Ni, B.J.; Yu, H.Q. Microbial Products of Activated Sludge in Biological Wastewater Treatment Systems: A Critical Review. *Crit. Rev. Environ. Sci. Technol.* **2012**, *42*, 187–223. https://doi.org/10.1080/10643389.2010.507696.
69. Kang, S.; Zhang, J.; Guo, X.; Lei, Y.; Yang, M. Effects of Ultrasonic Treatment on the Structure, Functional Properties of Chickpea Protein Isolate and Its Digestibility In Vitro. *Foods* **2022**, *11*, 880. https://doi.org/10.3390/foods11060880.
70. Xu, G. Analysis of Sewage Sludge Recovery System in EU-in Perspectives of Nutrients and Energy Recovery Efficiency, and Environmental Impacts. Master's Thesis, Norwegian University of Science and Technology, Taibei, Taiwan, 201; p. 88.
71. Cofie, O.; Kone, D.; Rothenberger, S.; Moser, D.; Zubruegg, C. Co-Composting of Faecal Sludge and Organic Solid Waste for Agriculture: Process Dynamics. *Water Res.* **2009**, *43*, 4665–4675. https://doi.org/10.1016/j.watres.2009.07.021.
72. Ammonia Volatilization Losses during Irrigation of Liquid Animal Manure. *Sustainability* **2019**, *11*, 6168. https://doi.org/10.3390/su11216168.
73. Qian, Y.; Sun, S.; Ju, D.; Shan, X.; Lu, X. Review of the State-of-the-Art of Biogas Combustion Mechanisms and Applications in Internal Combustion Engines. *Renew. Sustain. Energy Rev.* **2017**, *69*, 50–58. https://doi.org/10.1016/j.rser.2016.11.063.
74. Gahlot, P.; Balasundaram, G.; Tyagi, V.K.; Atabani, A.E.; Suthar, S.; Kazmi, A.A.; Kumar, A. Principles and Potential of Thermal Hydrolysis of Sewage Sludge to Enhance Anaerobic Digestion. *Environ. Res.* **2022**, *214*, 113856. https://doi.org/10.1016/j.envres.2022.113856.
75. Yuan, Y.; Liu, T.; Fu, P.; Tang, J.; Zhou, S. Conversion of Sewage Sludge into High-Performance Bifunctional Electrode Materials for Microbial Energy Harvesting. *J. Mater. Chem. A* **2015**, *3*, 8475–8482. https://doi.org/10.1039/C5TA00458F.
76. Abdu, N.; Abdullahi, A.A.; Abdulkadir, A. Heavy Metals and Soil Microbes. *Environ. Chem. Lett.* **2017**, *15*, 65–84. https://doi.org/10.1007/s10311-016-0587-x.